

Correlations of mixed systems in confining backgrounds

Mahdis Ghodrati^a

^a *Asia Pacific Center for Theoretical Physics, Pohang 37673, Republic of Korea*

E-mail: mahdis.ghodrati@apctp.org

ABSTRACT: We show that the entanglement of purification and the critical distance between the two mixed systems is a very powerful measure in probing phase structures of QCD and confining backgrounds as it can even distinguish the scale of chiral symmetry breaking versus the scale of confinement/deconfinement phase transitions. For two symmetric strips with equal and finite width and infinite length and in the background of several confining geometries, we numerically calculate the critical distance between them where the mutual information vanishes and show that this quantity can probe the very rich phase structures of these backgrounds. The geometries that we study here are AdS-soliton, Witten Sakai Sugimoto and deformed Sakai-Sugimoto, Witten-QCD, Klebanov-Strassler, Klebanov-Tseytlin, Klebanov-Witten, Maldacena-Nunez and Domain-Wall QCD model. For each background we also present the relation for the entanglement of purification. Finally, we show that the Crofton forms of these geometries also behave in a universal form where a well is being observed around the singularity point and therefore for all confining backgrounds, the Crofton form would also be capable of distinguishing the confining versus conformal backgrounds as it is also a tool in the reconstruction of various bulk geometries.

Contents

1	Introduction	1
2	Mixed correlation measures in confining backgrounds	3
3	Critical distances in the confining backgrounds	4
3.1	AdS soliton background	5
3.1.1	Other form of AdS soliton metric	8
3.2	Witten-Sakai-Sugimoto model	9
3.2.1	Deformed Sakai-Sugimoto	15
3.3	Witten-QCD	17
3.4	Klebanov-Strassler	19
3.5	Klebanov-Tseytlin	22
3.6	Klebanov-Witten	24
3.7	Maldacena-Nunez	25
3.8	Domain Wall AdS/QCD	26
4	Crofton form in confining backgrounds	30
4.1	AdS-soliton	30
4.2	Sakai-Sugimoto and deformed Sakai-Sugimoto	32
4.3	Klebanov-Strassler	34
4.4	Witten-QCD	34
4.5	Maldacena-Nunez	35
4.6	Klebanov-Tseytlin	35
4.7	Domain Wall QCD	35
5	Other holographic quantum measures in probing QCD phases	36
5.1	Quantum negativity in confining backgrounds	36
5.2	Calibrated geometry and bit threads in confining geometries	37
5.3	Holographic neutron stars and quantum information measures	39

1 Introduction

From the advent of Ryu-Takayanagi (RT) prescription [1] which for calculating the entanglement entropy of field theories uses calculations of the area of extremal surface which is homologous to the boundary, the deep connections between quantum information and geometry specially in the context of AdS/CFT has been ground in. The other new dualities in this context such as computational complexity/volume of the subregions [2–7], and

entanglement of purification(EoP)/minimal wedge cross section [8–10] further strengthened this connection.

As the calculations of the properties of geometrical objects in the bulk are much easier than the calculations of quantum measures in the boundary field theories and some of these geometrical objects can deeply probe the bulk and gather non-local information of it which would be dual to interesting quantum measures of the boundary, one would expect that these geometrical objects can also detect the rich phase structures of the exotic forms of matters such as quark gluon plasmas, strange metals, high temperature superconductors, superfluids, etc. The motivation of this work is to use minimal wedge cross section/EoP or mutual information between two mixed systems in the background of confining geometries to gain the properties of the phase structures of QCD.

We show in this work that the minimal wedge cross section of two symmetric strips which as proposed in [8] is dual to the entanglement of purification between the two mixed state, can capture a lot of information about the phase structures of various confining models. Specially this would be true for QCD and confining systems. Using the correlation measures of two symmetric mixed strips which would be easy to calculate, one could gain a lot about the phase structures of QCD and confining backgrounds, which is the motivation of this work. We found that in addition to the direct calculation of mutual information or minimal wedge cross section or EoP, in order to probe the phase structures of confining backgrounds, it would actually be easier and more preferable to calculate the critical distance between the two symmetric strips where the mutual information suddenly drops to zero. In addition, it could even detect the scale of chiral symmetry breaking and the confining-deconfining phase transitions which is the main result of this work.

For doing so we used several confining backgrounds. In general, these models are based on top-down and bottom-up structures. The top-down models of QCD use the fundamental models of string theory. For example the Witten model of low-energy QCD is constructed through the type-IIA supergravity. The boundary dual of this theory is a supersymmetric $4+1$ dimensional gauge theory which by higher temperatures dimensional reduction would lead to a non-supersymmetric QCD in $3+1$ dimension. This theory has a large number of colors and a large 't Hooft coupling. Extending this model, for instance, by adding flavor D8-branes, Sakai and Sugimoto could also explain the chiral symmetry breaking and its restoration at high temperatures by an interesting geometrical realization. The only free parameters in their model is the Kaluza-Klein mass parameter M_{KK} or u_{KK} and the 't Hooft coupling λ at that scale. Here, we study the behavior of several quantum information quantities such as entanglement entropy and mixed correlation measures such as entanglement of purification (EoP) and negativity versus these free parameters, such as u_{KK} , to probe the phase structures of QCD in these backgrounds. We hope it could also help to find the corrections needed to approach real QCD models at finite N_c and λ that could be gained from type-IIA string theory. Note that specifically since the Sakai-Sugimoto model, both qualitatively and quantitatively is very close to real QCD, our results in principle should be close to the results of lattice QCD.

Additionally, in any holographic QCD model, one would have an IR wall where the geometry would be terminated in the holographic direction, or there would be some sorts

of singularities there. In this work we also would like to check the effects of these soft or hard walls and cut-offs and the terminated radius u_{KK} on the quantum information measures such as mutual information, entanglement of purification and negativity, and the phase diagrams of various confining backgrounds. Therefore, another aim of this work is to check how the topology of different confining geometries would affect QCD properties and if/how the new holographic quantum measures such as entanglement of purification or quantum negativity, or the critical distance between two mixed systems, (and later complexity or complexity of purification), could probe these topological properties or dually the characteristics of QCD. This would actually be in continuation of our previous work [5], which we used complexity to probe the phase structures of Gubser's models of QCD [11], dubbed V_1 , V_2 , V_{QCD} and V_{IHQCD} . In the current work however, to construct the phase structure, we use new mixed correlations measures and new confining backgrounds, including AdS-soliton, Witten-Sakai-Sugimoto and deformed Sakai-Sugimoto, Witten-QCD, Klebanov-Strassler, Klebanov-Tseytlin, Klebanov-Witten, Maldacena-Nunez and domain-wall QCD. So, first in section 2, we show how to generalize the new quantum measures in confining backgrounds and then in section 3, we present the results for each of our confining models.

Then, in section 4, we present the relations and plots for the behavior of Crofton-from (which is a quantity in studying the Kinematic space and bulk reconstruction [12]) for each of these confining geometries and show they all have a universal behavior where a well could be detected around the singularity while it would become constant at the bigger holographic distances.

Finally, in section 5, we finish by discussions of how other quantum measures such as negativity or bit thread structures, could probe the phase diagrams of these QCD models and also distinguish their scale of chiral symmetry breaking versus the scale of confinement, and also how potentially these results could be employed in models of neutron stars to get further information about their compositions.

2 Mixed correlation measures in confining backgrounds

The generalization of entanglement entropy (EE) from conformal to non-conformal cases would be from

$$S_A = \frac{1}{4G_N^{(d+2)}} \int_{\gamma} d^d \sigma \sqrt{G_{\text{ind}}^{(d)}}, \quad (2.1)$$

to

$$S_A = \frac{1}{4G_N^{(10)}} \int d^8 \sigma e^{-2\phi} \sqrt{G_{\text{ind}}^{(8)}}, \quad (2.2)$$

where $G_N^{(d+2)}$ is the $d+2$ dimensional Newton constant and $G_{\text{ind}}^{(d)}$ is the induced string frame metric on γ . This generalization would be due to the fact that, in general, in the non-conformal theories, the volume of the $8-d$ compact dimensions and also the dilaton would be *non constant*.

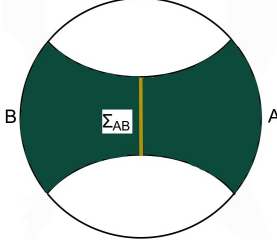


Figure 1. The minimal wedge cross section for the two connected mixed systems of A and B , i.e, Σ_{AB} is shown in yellow while the whole entanglement wedge is shown in green.

We put the setup of figure 1 in the background of confining geometries (as in figure 6 which is for the AdS soliton case) and probe various exotic features of these top-down, supergravity and confining backgrounds and show that mixed quantum entanglement measures and correspondingly the geometrical objects such as minimal wedge cross section can detect the effects of singularities, walls, throats and exotic topologies of such backgrounds.

The bulk minimal wedge cross section constructed from two mixed boundary regions, has been proposed in [8] to be dual to the entanglement of purification between these two mixed systems of A and B , as in figure 1. For the simple Schwarzschild AdS black brane geometry and for two regions with width of l and distance D , in [9], this quantity has been found as

$$\Gamma = \int_{z_D}^{z_{2l+D}} \frac{dz}{z^{d-1} \sqrt{1 - \frac{z^d}{z_h^d}}}, \quad (2.3)$$

where z_D and z_{2l+D} are the two turning points.

This then should be generalized for the non-conformal and specifically for confining geometry similar to the EE case. In fact, for several Dp-brane geometries, in [13], several similar quantum information measures have been calculated.

Here we could generalize it as

$$\Gamma = \int_{u_D}^{u_{2l+D}} du e^{-2\Phi} \sqrt{-\gamma_{ab}}. \quad (2.4)$$

This is because in non-conformal geometries, the dilaton field Φ and the volume of the compact dimensions are not constant and so similar to the entanglement entropy case, are needed to be considered for the formulation of the entanglement of purification as well.

3 Critical distances in the confining backgrounds

When the distance between two mixed systems becomes larger, at a specific critical distance D_c , the correlations, mutual information and entanglement of purification, between them vanish or rather drop to one order of magnitude lower.

For two equal strip with width l and distance D , the mutual information would be

$$I(D, l) = S_A + S_B - S_{AB} = 2S(l) - S(D) - S(2l + D), \quad (3.1)$$

and the critical distance can be found by where it drops to zero, i.e, $I(D_c, l) = 0$.

We show that this critical distance could give interesting new information about QCD phase structures as it in fact, would be a new scale in the theory.

The critical width for “one strip” could distinguish the confinement/deconfinement phase transition and it has been proposed that this critical width L_{crit} is proportional to the inverse of confinement temperature, i.e, $L_{\text{crit}} = \mathcal{O}(\Lambda_{IR}^{-1})$, where Λ_{IR} correspond to the singularity in each theory. However, here we can show that the critical distance between “two strips” is a stronger quantity and can even distinguish the scale of chiral symmetry breaking in addition to the confinement/deconfinement scale.

Similar to the work of [14], we find that the phase structure of confining background would be as shown in figure 2 and this then could be used to distinguish the scale of chiral symmetry breaking versus confinement/deconfinement phase transition. We present more numerical details about how this quantity would probe phase structures of QCD and could capture important scales in each theory.

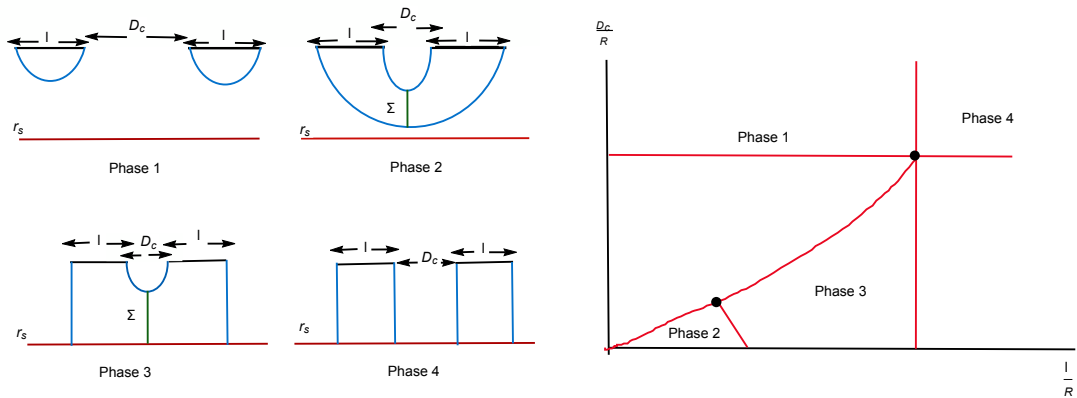


Figure 2. The structure of phases in confining backgrounds as first presented in [14].

3.1 AdS soliton background

The first background where we probe its phase structures using mixed correlations would be AdS soliton. This geometry was first introduced in the work of Myers and Horowitz [15] where the boundary CFT side have supersymmetry-breaking boundary conditions and the bulk geometry have negative energy dual to the negative Casimir energy in the boundary gauge theory side. Therefore, the AdS-soliton would have the lowest negative boundary energy among all solutions with the same asymptotic boundary. This negative energy which could source and generate the AdS-soliton geometry has been calculated as $\frac{E}{L_x^{n-2} L_y} \Big|_{\text{BH}} = \frac{(n-1)r_0^n}{2\ell^{n+1}}$, where n is the dimension of the boundary, $n+1$ is the dimension of the bulk geometry, L_x and L_y represent the extension of the surface on x and y directions and ℓ is the radius of AdS spacetime. In the bulk it means that all massive and massless particles would repel each other and therefore it means AdS-soliton would actually anti-gravitates.

The effects of this feature would then be carved in the structures of quantum states and on the behavior of quantum information measures, and bit threads structures.

In addition, since there are more phase transitions possible between AdS-black hole (BH) solutions and AdS-soliton geometry compared with other cases like AdS-BH and thermal AdS geometry, it would be more interesting to study the behaviors of mixed quantum information measures like entanglement of purification (EoP), mutual information (MI), complexity of purification (CoP), negativity, etc and also tools such as bit threads and Wilson loops during such phase transitions.

We choose the following background for the AdS soliton in the Poincare coordinates [16]

$$ds^2 = \frac{L_{\text{AdS}}^2}{z^2} \left(\frac{dz^2}{f(z)} + f(z)d\theta^2 - dt^2 + dr^2 + r^2 d\Omega_{d-3} \right), \quad (3.2)$$

where $f(z)$ is a harmonic function and has a general form as

$$f(z) = \left(1 - k_1 \frac{z}{z_0} \right) \left(1 - k_2 \frac{z}{z_0} \right) (1 + \sum_{n=1} c_n z^n). \quad (3.3)$$

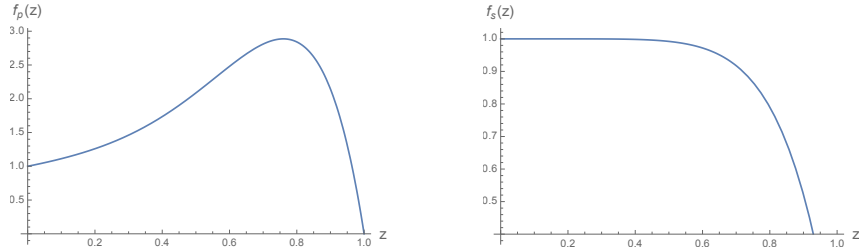


Figure 3. The behavior of $f_p(z)$ which uses the perturbative sum and arbitrary values of c_i as $k_1 = 1, k_2 = -2, c_1 = 1, c_2 = 2, c_3 = 3, c_4 = 4, c_5 = 5$, which is used for the general case of soliton is shown in the left part, and the function for the simplest AdS soliton case, $f_s(z) = 1 - (\frac{z}{z_0})^{8-d}$, $d = 1$ which we will use here for calculations is shown in the right part, in order to get intuitions about the metric of the AdS-soliton geometry.

By changing k_1 and k_2 , different IR behaviors could be yielded, but not for any k_1 and k_2 , this ansatz would become a solution of Einstein theory. In order to get a soliton AdS geometry one of the k_1 or k_2 should be negative, and the simplest AdS soliton would be with $k_1 = 1$ and $k_2 = -1$. The behaviour of $f(z)$ for the general case and simplest case are shown in figure 3. Here we take $f(z) = 1 - (\frac{z}{z_0})^{8-d}$ as for the simplest AdS soliton.

First, the width of the strip versus turning point z_t , for AdS soliton, could be found as

$$L(z_t) = \int_0^{z_t} \frac{2}{\sqrt{\left(1 - \left(\frac{z}{z_0} \right)^{8-d} \right) \left(\frac{z_t^6}{z^6} \frac{1 - \left(\frac{z_t}{z_0} \right)^{8-d}}{1 - \left(\frac{z}{z_0} \right)^{8-d}} - 1 \right)}}, \quad (3.4)$$

and the entanglement entropy for the connected solution in this background would be

$$S_C(z_t) = \int_0^{z_t} \frac{c_1}{z^3 \sqrt{1 - \frac{z^6 \left(1 - \left(\frac{z}{z_0}\right)^{8-d}\right)}{z_t^6 \left(1 - \left(\frac{z_t}{z_0}\right)^{8-d}\right)}}}, \quad (3.5)$$

and for the disconnected part one gets

$$S_D = - \int_0^{z_0} \frac{c_1}{z^3}, \quad (3.6)$$

where c_1 is just a constant combined of G_N , $G_N^{(10)}$, π , V_{d-3} , and is not important in our numerical studies here.

The behavior of these quantities are shown in figure 4. The noises observed in these phase diagrams could be due to various phenomena in the system such as presence of bound-entangled states, creation and annihilation of EPR pairs, etc.

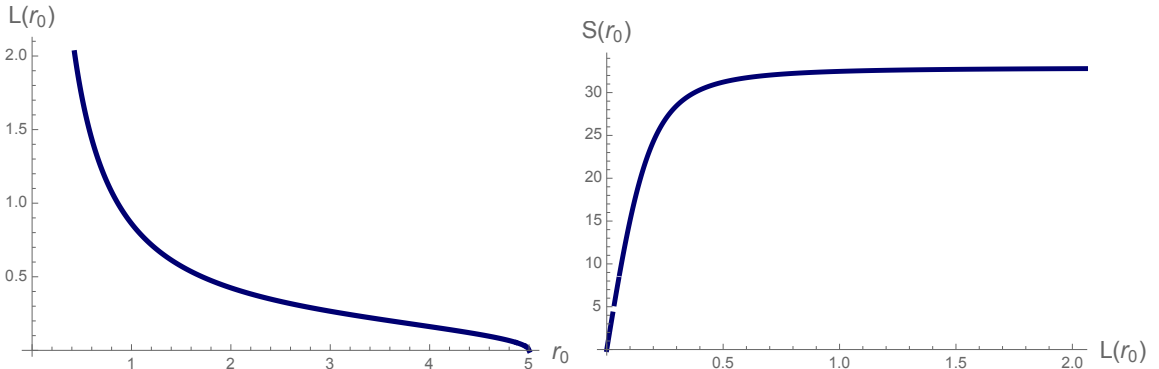


Figure 4. The relationship between width of a strip versus turning point τ_0 (in the left), and entanglement entropy versus L (in the right) in the AdS-soliton background.

Then, the position of singularity could be changed and the behavior of critical distance D_c versus the width l and therefore the phase structures of this theory could be found where the results are shown in figure 5. By changing z_0 at least four different phases could be detected here where in each phase the behavior of D_c is somehow distinct.

One important feature of this theory is the capping or the gap where its effect could be detected in the correlations, EoP and MI. As the entangling surface would wrap around the compact dimension, all the UV scaling structures specifically for the entanglement entropy and also entanglement of purification would become different. For instance EoP would be proportional to $\frac{L_\theta}{R} S_{UV}^{(d)}$ where L_θ is the fixed proper size of the compact circle, R is the linear size of the entangling surface and $S_{UV}^{(d)}$ is the UV structure of entanglement entropy of AdS_{d+1} . These measures in specific regimes and phases show monotonic RG flows as in c-theorem.

Note that AdS-soliton case could be presented in the cylinder or disc topologies. As mentioned in figure 1 of [16], the cylinder topology corresponds to the trivial product state

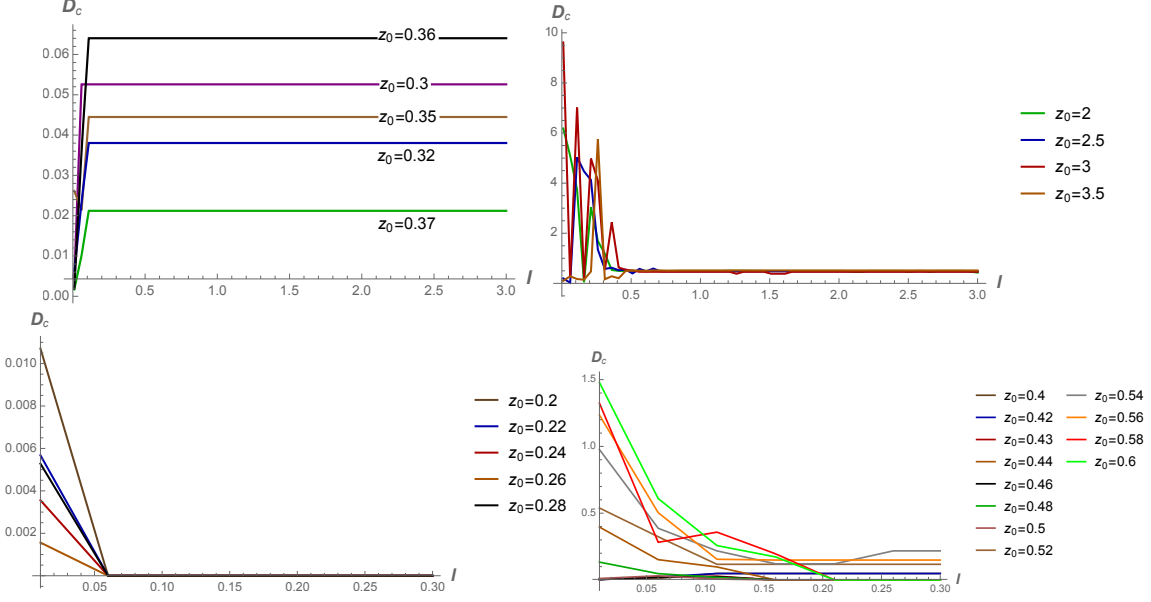


Figure 5. The four phases detected by the relationship between critical distance between two strips, D_c and width of the strip in AdS soliton background, for the range of parameter $0.35 < z_0 < 0.4$ in the up-left for the 1st phase and $2 < z_0 < 3.5$ in the up-right for the 2nd phase, $0.2 < z_0 < 0.3$ down-left in the 3rd phase and $0.4 < z_0 < 0.6$ down-right in the 4th phase which actually till $z_0 = 2$ would still be in the fourth phase.

after RG flow in MERA, and the disc topology corresponds to the entangled states protected by the symmetry or the topological orders. The critical distance in each case could capture these quantum distinctions as well.

Our results would also be very useful in studying the dynamics of black holes and also chaotic systems. In principle, the structures of islands and replica worm holes could also be investigated for the black holes in such confining backgrounds using this new quantity. Then, the interplay between the UV and IR correlations could also be probed this way.

3.1.1 Other form of AdS soliton metric

The AdS soliton can be written in other formats as well. One can write the general background which is asymptotically AdS as

$$ds^2 = \frac{r^2}{\ell^2} \left[- \left(1 - \frac{r_0^{p+1}}{r^{p+1}} \right) dt^2 + (dx^i)^2 \right] + \left(1 - \frac{r_0^{p+1}}{r^{p+1}} \right)^{-1} \frac{\ell^2}{r^2} dr^2, \quad (3.7)$$

where $i = 1, \dots, p$, which for certain values of p would arise in the near horizon geometry of p -branes. The energy here is $E_p = \frac{pV_p}{16\pi G_{p+2}\ell^{p+2}} r_0^{p+1}$.

The AdS soliton metric could then be derived by the analytical continuation $t \rightarrow i\tau$ and $x^p \rightarrow it$ and be written in the form of [15]

$$ds^2 = \frac{r^2}{\ell^2} \left[\left(1 - \frac{r_0^{p+1}}{r^{p+1}} \right) d\tau^2 + (dx^i)^2 - dt^2 \right] + \left(1 - \frac{r_0^{p+1}}{r^{p+1}} \right)^{-1} \frac{\ell^2}{r^2} dr^2, \quad (3.8)$$

where there are $p - 1$ x^i 's. The energy then would be $E = -\frac{r_0^{p+1}\beta V_{p-1}}{16\pi G_{p+2}\ell^{p+2}}$, where $\beta = 4\pi l^2/(p+1)r_0$ is the period.

In order to understand this negative energy feature of the AdS soliton, in [17], the geodesic motions of massive and massless particles have been studied in this background. In the Poincare coordinate, the metrics have been written as

$$\begin{aligned} \text{AdS-BH} : \quad & ds^2 = \frac{r^2}{\ell^2}(-h d\eta^2 + d\vec{x} \cdot d\vec{x} + dy^2) + \frac{\ell^2 dr^2}{r^2 h}, \\ \text{AdS-soliton} : \quad & ds^2 = \frac{r^2}{\ell^2}(+h dy^2 + d\vec{x} \cdot d\vec{x} - d\eta^2) + \frac{\ell^2 dr^2}{r^2 h}, \end{aligned} \quad (3.9)$$

where $h = 1 - \frac{r_0^n}{r^n}$. In that work the topologies of AdS-BH and AdS-soliton has been compared, as in figure 6, where the horizon surface of AdS-BH has the topology of R^{n-} , but the $r = r_0$ “line” in AdS-soliton case has the topology of $R^{n-2,1}$. The two mixed systems in the form of two parallel strips with width l and infinite lengths would be located on the boundary side.

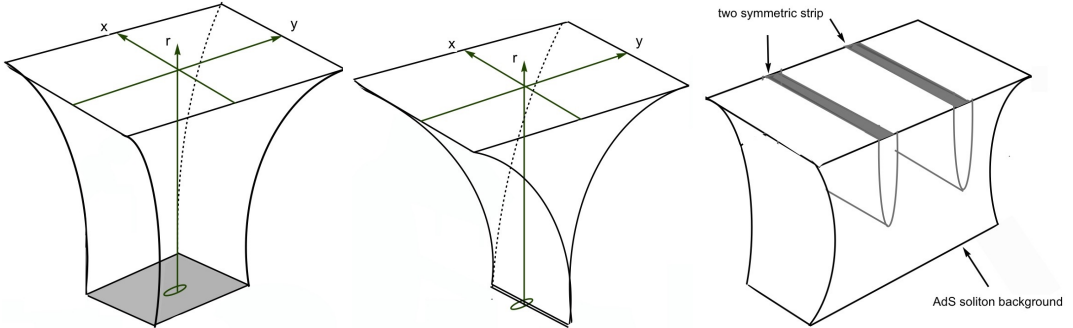


Figure 6. The picture in the left is the AdS-BH solution, the one in the middle is an AdS-soliton geometry and the one in the right shows our system of two symmetric strips in the AdS soliton background.

Note that in AdS/CFT setup, and for the AdS soliton case, the cold and large black holes are dual to the deconfining phase and the hot and small black holes are dual to the confining phase.

3.2 Witten-Sakai-Sugimoto model

In this work we are more interested in the top-down holographic QCD models which are engineered by intersecting D-branes, like D4-D8 brane intersections known as Witten-Sakai-Sugimoto model shown in figure 7. This theory in fact can nicely model the $SU(N_f)_L \times SU(N_f)_R$ chiral flavor symmetry breaking.

In this setup, x^4 is the spatial coordinate which is being compactified on S^1 , which for fermions would have anti-periodic boundary conditions. The gauge theory is coupled to N_f left-handed quarks and N_f right-handed quarks which are localized at different points of the compact circle. The D8-branes are at $x^4 = 0$ and the anti-D8 branes are located in parallel and at $x^4 = \pi R$, and R is the radius of S^1 .

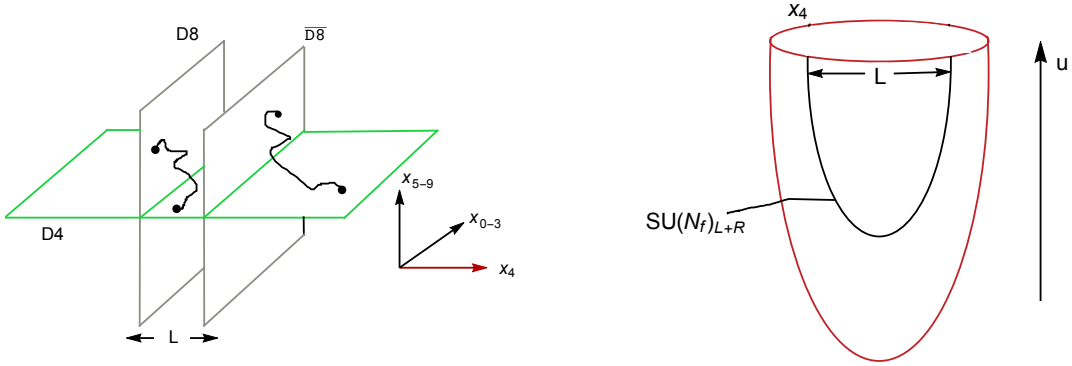


Figure 7. Intersecting D4-D8 brane model of Witten-Sakai-Sugimoto. Usually the D8-branes are treated as probe branes.

In the above picture, the D4-branes correspond to color sector and the open strings which end on them produce the color/gluon gauge field. On the other hand, the D8-branes are flavor branes and the strings ending on them give the flavor/meson gauge field. The strings which are stretched between D4 and D8 branes would then give rise to the quarks. The closed strings also correspond to the glue-balls. Using this picture, the color/flavor duality would then map to open/closed string duality.

The entanglement and correlation structures among D8-D8, D4-D4 and D8-D4 branes would be different. The different correlation measures could then probe all these structures which we for the first step, we show that it can be captured first by the critical distance D_c .

The metric of D4-branes is

$$ds_{D4}^2 = \left(\frac{u}{R_{D4}} \right)^{3/2} (-dt^2 + \delta_{ij}dx^i dx^j + f(u)(dx^4)^2) + \left(\frac{R_{D4}}{u} \right)^{3/2} \left(\frac{du^2}{f(u)} + u^2 d\Omega_4^2 \right), \quad (3.10)$$

where the dilaton, the Ramond-Ramond field, the function $f(u)$ and the AdS radius are defined as

$$e^\phi = g_s \left(\frac{u}{R_{D4}} \right)^{3/4}, \quad F_4 \equiv dC_3 = \frac{2\pi N_c}{V_4} \epsilon_4, \quad f(u) \equiv 1 - \frac{u_{KK}^3}{u^3}, \quad R_{D4}^3 \equiv \pi g_s N_c l_s^3. \quad (3.11)$$

Here, N_c is the number of colors in the gauge group, g_s is the string coupling, l_s is the string length which has the relation $l_s^2 = \alpha'$, V_4 is the volume of the unit four sphere S^4 , and s_4 is the volume form of S^4 . In addition, u is the holographic radial direction, which is in the region $u_{KK} \leq u \leq \infty$.

Then, assuming the position of D8 brane at $x^4 = 0$ and anti-brane at $x^4 = \pi R$, leading to relation $dx^4/du = 0$, the induced metric of the D8-brane becomes

$$ds_{D8}^2 = \left(\frac{u}{R_{D4}} \right)^{3/2} (-dt^2 + \delta_{ij}dx^i dx^j) + \left(\frac{R_{D4}}{u} \right)^{3/2} \left(\frac{du^2}{f(u)} + u^2 d\Omega_4^2 \right). \quad (3.12)$$

As there are two metrics, one for D4-branes and one for D8 branes, here one might be confused that which one should be employed to calculate the holographic mixed quantum measures. In fact, the calculations should be done for the flavor D-branes metric which represent the quark sector, which here for the case of Sakai-Sugimoto, would correspond to the *D8-branes*. In works such as [18], for calculating the pair production rates, also the imaginary part of D8-branes have been evaluated, which again is the main part for mixed correlations too. Therefore, for the calculation of Sakai-Sugimoto case, we consider the above metric 3.12.

We find $S_C(u_t)$, i.e, entanglement entropy at turning point u_t of the strip with width $L(u_t)$ as

$$S_C(u_t) = \frac{V_3 V_4 R_{D_4}^3}{2g_s^2 G_N^{(10)}} \int_{u_t}^{\infty} du \frac{u}{\sqrt{\left(1 - \frac{u_{KK}^3}{u^3}\right) \left(1 - \frac{u_t^5}{u^5}\right)}}, \quad (3.13)$$

and the width of the strip in terms of turning point as

$$L(u_t) = 2R_{D_4}^{\frac{3}{2}} \int_{u_t}^{\infty} du \frac{1}{\sqrt{u^3 \left(1 - \frac{u_{KK}^3}{u^3}\right) \left(\frac{u^5}{u_t^5} - 1\right)}}. \quad (3.14)$$

The plot of $L(u_t)$ versus turning point u_t and entanglement entropy versus L is shown in figure 8.

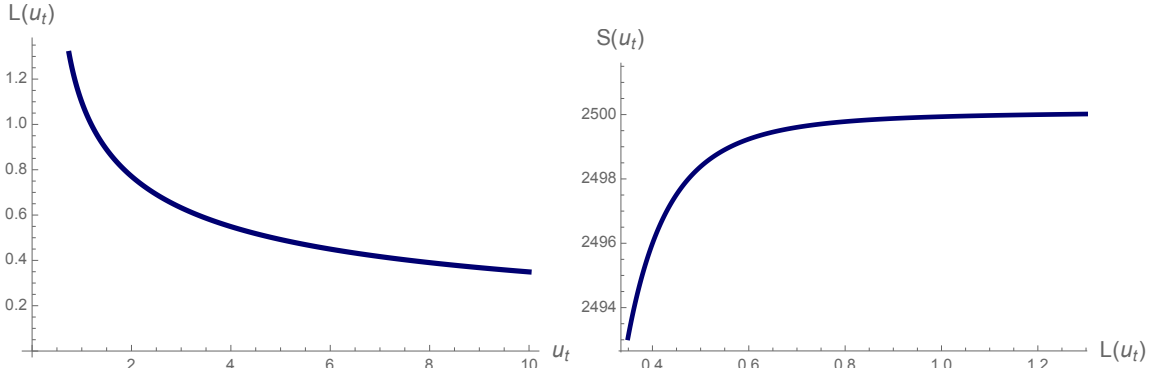


Figure 8. The plot of $L(u_t)$ vs. turning point u_t and $S(u_t)$ vs. $L(u_t)$ for the case of Sakai-Sugimoto, for $u_{KK} = 0.5$.

Next, in this confining model, we would like to examine the behavior of critical distance between the two strips D_c as a function of u_{KK} and detect various phases in this specific background.

Again, at least four distinct phases could be detected. In the first phase shown in figure 9, increasing u_{KK} would increase D_c . When u_{KK} becomes zero the critical distance would be around $D_c = 0.899$. The upper bound for u_{KK} in this phase is $u_{KK} = 0.5$ corresponding to $D_c = 0.97$. After that increasing u_{KK} decreases D_c and we enter the next phase which by increasing u_{KK} , D_c would decrease.

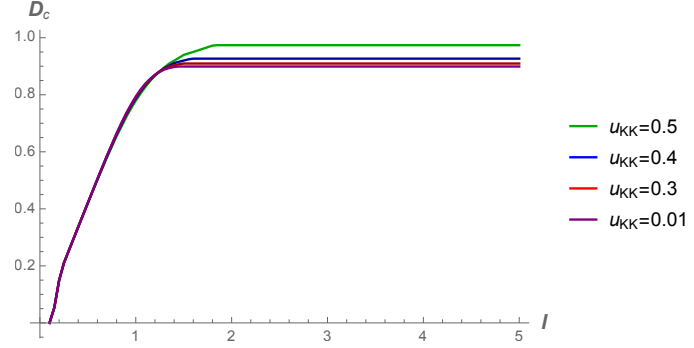


Figure 9. The plot of D_c vs. l for different u_{KK} in phase 1.

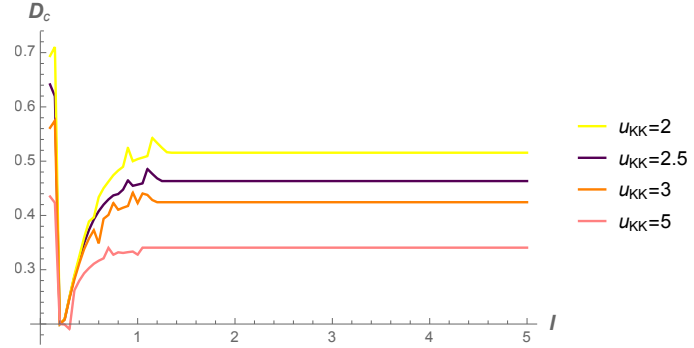


Figure 10. The plot of D_c vs. l for different u_{KK} in phase 2.

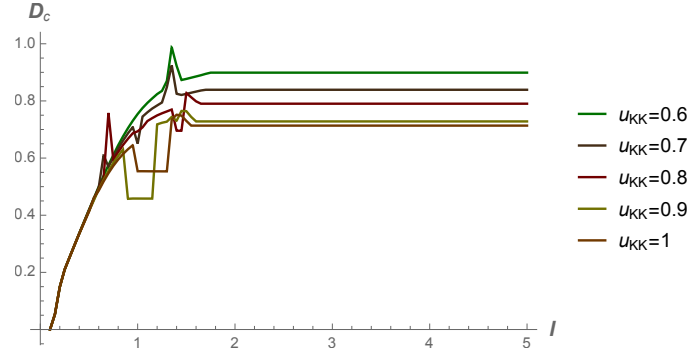


Figure 11. The plot of D_c vs. l for different u_{KK} in phase 3.

In the second phase, shown in figure 10, one could note that increasing u_{KK} would decrease critical distance D_c unlike the previous phase of figure 9.

In the third phase shown in figure 11, again one can see that after reaching its maximum at the previous phase, increasing u_{KK} decreases D_c . In figure 12 we show all three phases that appear first.

In figure 13, we show in more details the behaviour of critical distance D_c at various u_{KK} for a constant l . Ignoring various physical constant one could observe in figure 13 that the first phase transition occurs around $u_{KK} = 0.5$ and then the next one around $u_{KK} = 3.5$

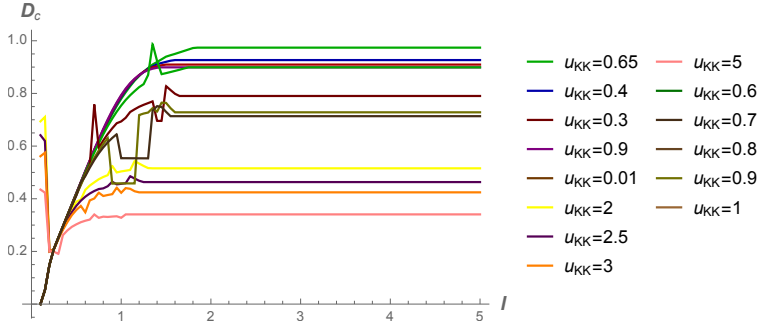


Figure 12. Three of the four phases of 2 is shown here.

and the third one around $u_{KK} = 12$, and the last one around $u_{KK} = 16$ where after that D_c becomes asymptotically zero. So one of these phase transitions is related to chiral symmetry breaking/restoration for the massless quarks and the other sharp phase transition is due to the confinement/deconfinement transition related to the breaking/restoring of Z_{N_c} global symmetry. Note that as found in [19], the chiral symmetry would be broken in the confined phase, so the first phase transition seen in figure 13 is due to the chiral symmetry breaking and the second one due to the deconfinement and the last one is due to the drop in the order of magnitude of the mutual information.

So both the confinement and approximate spontaneous chiral symmetry breaking would affect the correlations between mixed systems in these confining backgrounds where mutual information and other mixed correlation measures such as entanglement of purification (and probably complexity of purification) could detect their effects.

Note that in this background, the massless fields living on the D8-branes would lead to the low-spin mesons, while the strings which fall from the D8-branes down to the wall at $u = u_{KK}$ and then going back up again would lead to the higher spin mesons. This is another reason that changing the position of $u = u_{KK}$ would have such a strong effect on the entanglement and correlations between two mixed systems in this confining background as we have observed in figures 9, 10, 11 and 12. Also, this change of position of u_{KK} would change the behavior of the fluctuations of the gauge fields on the branes which are responsible for the creation of pseudo-vectors, scalar mesons and massless pions. These particles could also mediate information between the two mixed systems and therefore affect the phase structures of QCD probing by these quantum measures.

These phase transitions could also be examined from the point of view of traversable wormholes [20, 21]. During these first order phase transitions, the traversable wormholes would exchange their configurations. Also, it could be seen as Hawking-Page-like phase transition where the quark-anti-quark potential changes from the linear behavior in the low-temperature and finite values of $\sqrt{g_{tt}g_{xx}}$ and the free energy of the order N_c^0 in the confined phase to the decaying potential in higher temperatures and zero value of $\sqrt{g_{tt}g_{xx}}$, and free energy of the order N_c^2 in the deconfined phase.

In [5], we also established the connections between complexity and potential in the QCD models. The similarities between the behavior of potential and entanglement and

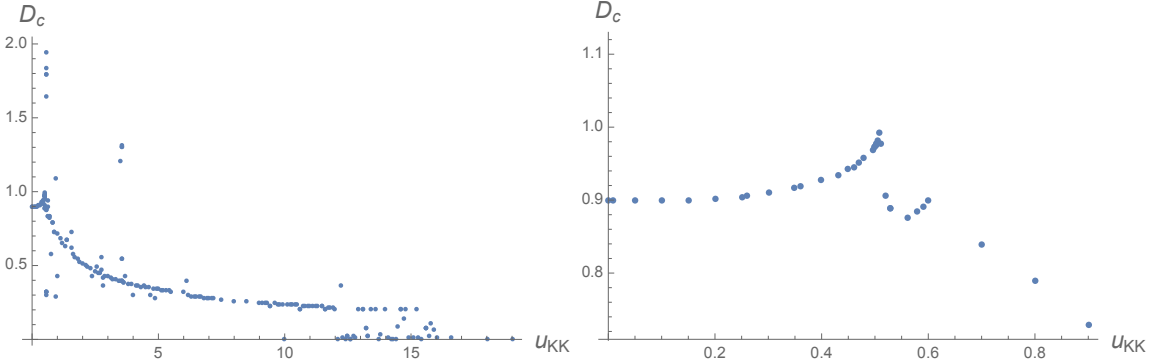


Figure 13. The plots of D_c vs. u_{KK} which the one in the left shows the whole four phases mentioned in figure 2 and the one in the right shows the first phase more clearly.

complexity of purification could also be observed in these confining models, specifically in Sakai-Sugimoto and Klebanov-Strassler case.

One should note that as mentioned in [19], in these confining backgrounds there is another critical separation denoted by L_c where when the quark separation is $L > L_c \simeq 0.97 * R$ the chiral symmetry would be restored at the temperature $T_d = 1/2\pi R$, and when $L < L_c \simeq 0.97 * R$ in an intermediate deconfined phase, the chiral symmetry is broken and again the chiral symmetry would be restored at $T_{\chi SB} \simeq 0.154/L$. Here R is the radius of the circle where the $4 + 1$ supersymmetric gauge theory is compactified on. Note also that here all the phase transitions are first order.

The competitions between chiral symmetry breaking/restoration and the vanishing of mutual information due to increasing the distance between the two strips would in fact create the four phase transitions also observed in 12 and 13. In general the scale of chiral symmetry breaking and confinement would be independent, as the scale of chiral symmetry breaking would mostly depend on the distance between D8-branes or the fermions on the compactified circle, while the scale of confinement would depend on the radius where D4-brane is wrapped around, or the radius of the circle which the $SU(N_c)$ gauge theory is compactified on it.

So in the Sakai-Sugimoto model, the chiral symmetry breaking/restoration which is related to the mass scale of mesons, $(\frac{1}{L})$, is related to the distance between D8 branes. More precisely, the low spin mesons are described by strings attached between the two D8 branes while the high spin mesons fall from D8 branes on the wall at $u = u_{KK}$, being completely stretched on the wall and then go back to the D8 brane. The confinement/deconfinement phase transition happens at the scale which is related to the mass of glueballs, $\frac{1}{R}$, which is related to the radius where D4 brane is wrapped around.

Also, note that in this model, the unstable modes have been observed and studied in the literature which specifically in high-energy regimes could significantly affect the quantum measures that we use here.

The relation for the minimal wedge cross section could be found using the relation

$$\Gamma_{WSS} = R_{D4}^3 \int_{u_D}^{u_{2l+D}} du \frac{u^5}{1 - \frac{u_{KK}^3}{u^3}}. \quad (3.15)$$

Based on the AdS/CFT dictionary we have relations between the parameters M_{KK} , g_{YM} , N_c in the boundary gauge side and R_{D4} , u_{KK} , g_s in the gravity side as

$$R_{D4}^3 = \frac{1}{2} \frac{\lambda l_s^2}{M_{KK}}, \quad u_{KK} = \frac{2}{9} \lambda M_{KK} l_s^2, \quad g_s = \frac{1}{2\pi} \frac{\lambda}{M_{KK} N_c l_s}. \quad (3.16)$$

The 't Hooft coupling λ is $\lambda = g_{YM}^2 N_c$ and the gauge coupling g_{YM} at the cutoff scale M_{KK} can be written as $g_{YM}^2 = (2\pi)^2 g_s l_s / \delta x^4$ and also we have the relation $M_{KK} \equiv \frac{2\pi}{\delta x^4}$ [18].

It could be seen that the string coupling g_s , the number of colors of gauge group N_c , the string length l_s and the cutoff energy M_{KK} increase the entanglement of purification while the periodicity of the boundary condition δx^4 would have an inverse effect and decreases the EoP. The increasing behavior of EoP versus M_{KK} and its decrease versus δx^4 are shown in figure 14.

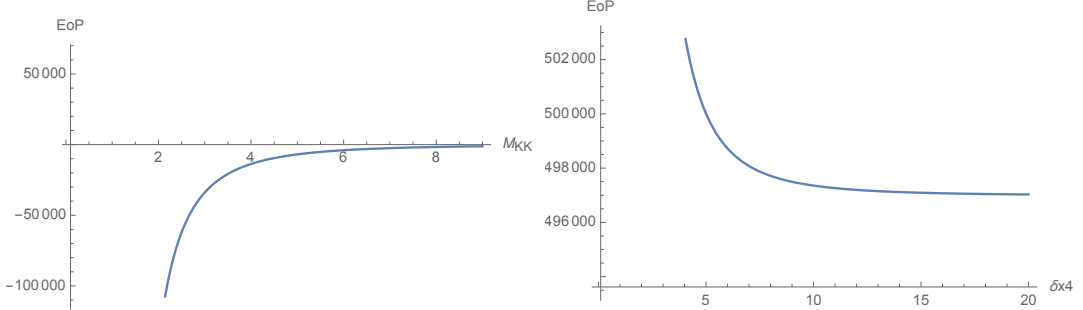


Figure 14. The behavior of entanglement of purification versus M_{KK} and δx_4

3.2.1 Deformed Sakai-Sugimoto

One can then consider the deformed Sakai-Sugimoto geometry [18, 19], where x^4 instead of being constant, depends on the coordinate u .

It has the configuration as shown in figure 15 and its metric is as follows

$$ds_{D8}^2 = \left(\frac{u}{R_{D4}} \right)^{3/2} (-dt^2 + \delta_{ij} dx^i dx^j) + \left(\frac{u}{R_{D4}} \right)^{3/2} \frac{du^2}{h(u)} + \left(\frac{R_{D4}}{u} \right)^{3/2} u^2 d\Omega_4^2, \quad (3.17)$$

where

$$h(u) \equiv \left[f(u) \left(\frac{dx^4(u)}{du} \right)^2 + \left(\frac{R_{D4}}{u} \right)^3 \frac{1}{f(u)} \right]^{-1}. \quad (3.18)$$

The entanglement entropy of a strip in terms of the turning point is

$$S(u_t) = \frac{V_3 V_4 R_{D4}^3}{2g_s^2 G_N^{(10)}} \int_{u_t}^{\infty} du \frac{u}{\sqrt{(1 - \frac{u_{KK}^3}{u^3})(1 - \frac{u_t^5}{u^5})}} + \frac{V_3 V_4 R_{D4}^{\frac{3}{2}}}{2g_s^2 G_N^{(10)}} \int_{u_t}^{\infty} du \left(\frac{dx^4(u)}{du} \right) \sqrt{\frac{u^5(1 - \frac{u_{KK}^3}{u^3})}{1 - \frac{u_t^5}{u^5}}}. \quad (3.19)$$

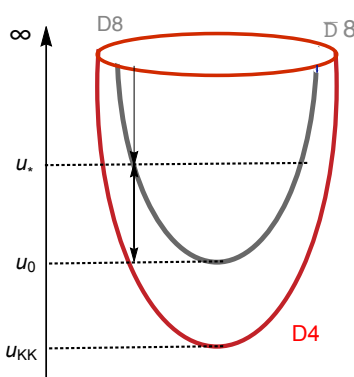


Figure 15. The geometry of deformed Sakai-Sugimoto.

Note that the first term is similar to the previous usual Sakai-Sugimoto case, while in the deformed case the second term is added which increases the entanglement entropy compared to the previous case of relation 3.13. The gradient of the coordinate $x^4(u)$ versus u controls the difference.

Similarly, the width of the strip versus the turning point u_t could be written as

$$L(u_t) = 2R_{D4}^{\frac{3}{2}} \int_{u_t}^{\infty} du \frac{1}{\sqrt{u^3 \left(1 - \frac{u_{KK}^3}{u^3}\right) \left(\frac{u^5}{u_t^5} - 1\right)}} + 2 \int_{u_t}^{\infty} du \left(\frac{dx^4(u)}{du}\right) \sqrt{\frac{1 - \frac{u_{KK}^3}{u^3}}{\frac{u^5}{u_t^5} - 1}}, \quad (3.20)$$

which again the second term has been added to the previous case of relation 3.14.

For this case then, the relation for the minimal wedge cross section would be

$$\Gamma_{\text{Deformed SS}} = R_{D4}^3 \int_{u_D}^{u_{2l+D}} du \frac{u^5}{1 - \frac{u_{KK}^3}{u^3}} + \int_{u_D}^{u_{2l+D}} du u^8 \left(1 - \frac{u_{KK}^3}{u^3}\right) \left(\frac{dx^4(u)}{du}\right)^2. \quad (3.21)$$

So again in the deformed case the second term is being added. Therefore, the minimal wedge cross section of deformed Sakai-Sugimoto is bigger than the normal case, or rather the entanglement of purification of two mixed system is higher and the difference is being controlled by the derivative of $x^4(u)$ relative to u .

By calculating the DBI action and then calculating its Hamiltonian which is conserved one would specifically get the relation for $u' = du/dx^4$ [19] as

$$u'^2 = f^2(u) \left(\frac{u}{R_{D4}}\right)^3 \left(\frac{f(u)}{f(u_0)} \frac{u^8}{u_0^8} - 1\right), \quad (3.22)$$

Then, we can insert the inverse of this relation into all the previous results for the deformed Sakai-Sugimoto and find the numerical solutions for this case as well. However, since the second integral contains a square term, the numerical solutions become much more complicated and noisy, and we leave its direct calculations for the future works.

3.3 Witten-QCD

In the string frame, the metric of Witten-QCD and its dilaton field is written as [22],

$$ds^2 = \left(\frac{u}{R}\right)^{3/2} \left(\eta_{\mu\nu} dx^\mu dx^\nu + \frac{4R^3}{9u_t} f(u) d\theta^2 \right) + \left(\frac{R}{u}\right)^{3/2} \frac{du^2}{f(u)} + R^{3/2} u^{1/2} d\Omega_4^2,$$

$$f(u) = 1 - \frac{u_t^3}{u^3}, \quad R = (\pi N g_s)^{\frac{1}{3}} \alpha'^{\frac{1}{2}}, \quad e^\Phi = g_s \frac{u^{3/4}}{R^{3/4}}. \quad (3.23)$$

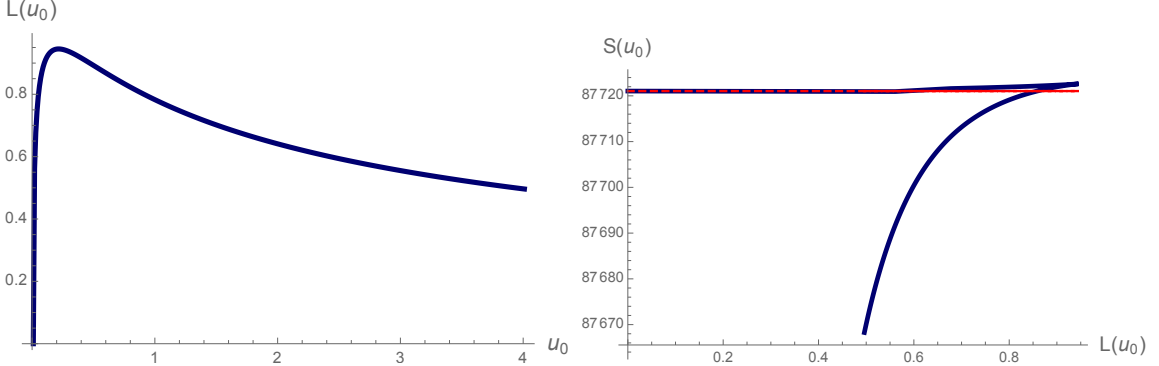


Figure 16. The relationship between width of a strip versus turning point τ_0 (in the left), and entanglement entropy versus L (in the right) in the background on Witten-QCD.

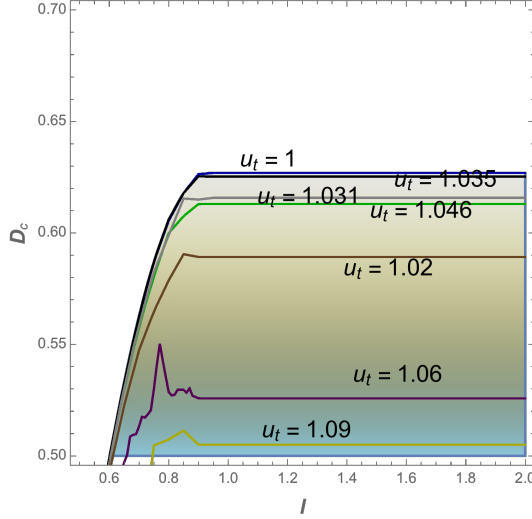


Figure 17. The behaviour of D_c vs l for various u_t is shown where the region for non-zero mutual information for each parameter is the region covered below each curve.

The turning point of the RT surface depends on the width of the strip $L(u_0)$ and has been found in [23] as

$$L(u_0) = 2 \int_{u_0}^{\infty} du \sqrt{\frac{\left(\frac{R}{u}\right)^3 \frac{1}{f(u)}}{\frac{f(u)u^5}{f(u_0)u_0^5} - 1}}, \quad (3.24)$$

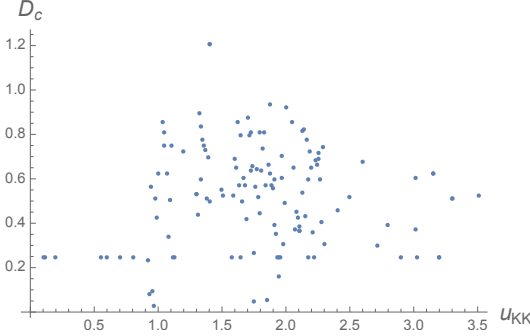


Figure 18. Data points of D_c vs u_{KK} in Witten background.

and the entropy of the connected solution S_C would be [23]

$$S_C(u_0) = \frac{V_2}{G_N^{(10)}} \frac{8\pi^2 R^{\frac{9}{2}}}{9g_s^2 \sqrt{u_t}} \int_{u_0}^{\infty} du \sqrt{\frac{u^2}{1 - \frac{u_0^5}{u^5} \frac{f(u_0)}{f(u)}}}. \quad (3.25)$$

Using the above relations, the phase structures can be numerically probed where the results are shown in figures 17 and 18. Note that specifically in figure 18, the first phase is when D_c versus u_{KK} is constant, then around $u_{KK} = 1$ there is a drop and then a singularity or rather a jump which is the second phase, then another one around $u_{KK} = 1.3$ and the next around $u_{KK} = 1.7$, and then D_c decreases by increasing u_{KK} which is the last phase, a similar behavior to AdS-soliton case.

As the numerics are very sensitive to u_t , however, the diagrams jump from higher to lower and the results are rather noisy. However, interestingly in some works such as [24], it has been shown that in holographic models of QCD, a Chern-Simons coupling between the vector and axial-vector mesons could be predicted which this coupling could mix the transverse polarization states, ρ and a_1 , and it produces instabilities which could be one of the reasons of the noises we observed here. Note that this Chern-Simons term does not depend on the metric and in general, it is present in any holographic dual description of QCD, and therefore in principle it is one of the reasons of the noises observed here, in all of our confining models. There could also be some interplay between this condensation and other effects such as pion condensation, chiral symmetry breaking, color superconductivity, mixed polarization states, etc, which could affect the behavior of these quantum measures in various phases.

Also, another reason for seeing these sharp jumps is due to the fact that the quarks are considered massless in these models which would make the chiral symmetry breaking/restoration a sharp one as the chiral condensate acts as an order parameter, and also for the case of confinement phase transition, the quarks could be ignored and so the breaking of Z_{N_c} global symmetry would cause another jump.

Then, if we use relation 2.4, for this case, the minimal wedge cross section Γ would be

found as

$$\Gamma_{\text{WQCD}} = \int_{u_D}^{u_{2l+D}} du \frac{2R^{9/2}u}{3u_0^{1/2}g_s^2}, \quad (3.26)$$

which its relation with various parameters of the theory could be seen.

3.4 Klebanov-Strassler

Another interesting geometry worths to study and check the behaviour of quantum information measures and D_c in it, would be the Klebanov-Strassler (KS) case [25]. This type-IIB supergravity solution has various fluxes and warp factors and are dual to the confining $\mathcal{N} = 1$ SYM theories which describe the baryonic branch of the dual gauge theory.

The KS metric is actually being constructed by the collection of N regular and M fractional D3-branes in the geometry of the deformed conifold. The fractional D3-branes could be thought as D5-branes that wrap the two-cycle of $T^{1,1}$ which collapse at the apex $\tau = 0$ in a way that the world-volume would effectively becomes that of a 3-brane.

There are two free parameters in the KS model which the dual interpretations of them are baryonic VEV and the gauge coupling constant. The Maldacena-Nunez solution which we study later, could also be considered as the end point of a flow from KS by changing these two parameters.

The gauge group on the stack of N D3-branes and M fractional D3-branes is $SU(N + M) \times SU(N)$ [26]. The limit where $M \ll N$ corresponds to the Klebanov-Tseytlin solution which we also check later.

The fluxes follow the relations

$$\int_{T^{1,1}} F_5 \propto N, \quad \int_{S^3} F_3 \propto M, \quad (3.27)$$

and the NSNS-flux would be

$$H_3 \propto \frac{g_s M}{\tau} d\tau \wedge \omega_2, \quad \text{therefore: } \int_{S^2} B_2 = g_s M \log(\tau/\tau_0), \quad (3.28)$$

where ω_2 is the volume form of the two-sphere of $T^{1,1}$ and τ_0 is just an integration constant.

The form of the metric is

$$ds_{\text{def}}^2 = \frac{1}{2} \epsilon^{\frac{4}{3}} K \left[\frac{1}{3K^3} (d\tau^2 + g_5^2) + \sinh^2\left(\frac{\tau}{2}\right) (g_1^2 + g_2^2) + \cosh^2\left(\frac{\tau}{2}\right) (g_3^2 + g_4^2) \right], \quad (3.29)$$

and K is a decreasing function of the radial coordinate τ , as

$$K(\tau) = \frac{(\sinh 2\tau - 2\tau)^{\frac{1}{3}}}{2^{\frac{1}{3}} \sinh \tau}. \quad (3.30)$$

For these confining geometries which has an exotic throat as shown in figure 19, the tools of bulk reconstruction such as Kinematic space, Crofton form, tensor networks or even the form of bit threads or “quantum bit threads” [27, 28], entanglement contours and Page curves could give further information about the interplay between geometry and topology

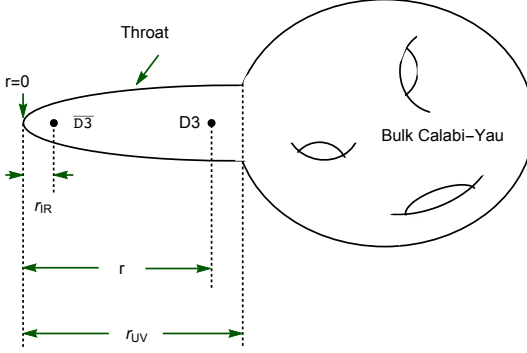


Figure 19. Klebanov-Strassler is the part of the warped throat in this geometry.

in the bulk, and the information in the boundary. The complicated relation for the Crofton form of KS metric is presented in equation 4.3.

The Klebanov-Strassler (KS) metric which is known also as warped deformed conifold is obtained by a collection of N regular and M fractional D3-branes [25].

The metric is

$$ds_{10}^2 = h^{-\frac{1}{2}}(\tau) dx_\mu dx^\mu + h^{\frac{1}{2}}(\tau) ds_6^2, \quad (3.31)$$

where again the ds_6^2 is the metric of the deformed conifold which is

$$ds_6^2 = \frac{1}{2} \epsilon^{\frac{4}{3}} K(\tau) \left[\frac{1}{3K^3(\tau)} (d\tau^2 + (g^5)^2) + \cosh^2\left(\frac{\tau}{2}\right) [(g^3)^2 + (g^4)^2] + \sinh^2\left(\frac{\tau}{2}\right) [(g^1)^2 + (g^2)^2] \right]. \quad (3.32)$$

The parameters of the metric are

$$\begin{aligned} K(\tau) &= \frac{(\sinh(2\tau) - 2\tau)^{\frac{1}{3}}}{2^{\frac{1}{3}} \sinh \tau}, & h(\tau) &= (g_s M \alpha')^2 2^{2/3} \epsilon^{-8/3} I(\tau), \\ I(\tau) &= \int_{\tau}^{\infty} dx \frac{x \coth x - 1}{\sinh^2 x} (\sinh(2x) - 2x)^{\frac{1}{3}}, \end{aligned} \quad (3.33)$$

and

$$\begin{aligned} g^1 &= \frac{1}{\sqrt{2}} [-\sin \theta_1 d\phi_1 - \cos \psi \sin \theta_2 d\phi_2 + \sin \psi d\theta_2], & g^2 &= \frac{1}{\sqrt{2}} [d\theta_1 - \sin \psi \sin \theta_2 d\phi_2 - \cos \psi d\theta_2], \\ g^3 &= \frac{1}{\sqrt{2}} [-\sin \theta_1 d\phi_1 + \cos \psi \sin \theta_2 d\phi_2 - \sin \psi d\theta_2], & g^4 &= \frac{1}{\sqrt{2}} [d\theta_1 + \sin \psi \sin \theta_2 d\phi_2 + \cos \psi d\theta_2], \\ g^5 &= d\psi + \cos \theta_1 d\phi_1 + \cos \theta_2 d\phi_2. \end{aligned} \quad (3.34)$$

Note that $h(\tau)$ is the warp factor here. Also, as mentioned, ds_6^2 is the deformed conifold which is a cone over S space that is topologically $S^3 \times S^2$. The (g_1, g_2) would build the S^2 part which shrinks to zero size at the apex of the deformed conifold while (g_3, g_4, g_5) build the S^3 part which have a finite size.

In [29], it has been mentioned that the IR behaviour of the function I acts as $I(\tau \rightarrow 0) \rightarrow a_0 - a_2 \tau^2 + \mathcal{O}(\tau^4)$, and since there is no linear term in τ , the expansion is really around the end of space and the Wilson loop would find it more favorable to arrange themselves there. This point then should show its effects on the behaviours of other quantum information measures such as entanglement of purification, mutual information and negativity for the two strips in the mixed setup as we examine here.

The length of the strip versus turning point of the RT surface can be written as [9]

$$L(\tau_0) = \frac{2^{\frac{5}{6}} \epsilon^{\frac{2}{3}}}{\sqrt{3}} \int_{\tau_0}^{\infty} d\tau \frac{\sinh(\tau)}{(\sinh(2\tau) - 2\tau)^{\frac{1}{3}}} \sqrt{\frac{h(\tau)}{\frac{\sinh^2(\tau)}{\sinh^2(\tau_0)} \left(\frac{\sinh(2\tau) - 2\tau}{\sinh(2\tau_0) - 2\tau_0}\right)^{\frac{2}{3}} - 1}}, \quad (3.35)$$

and the entanglement entropy for the connected solution is

$$S_C(\tau_0) = \frac{V_2 \pi^3 \epsilon^4}{3G_N^{(10)}} \int_{\tau_0}^{\infty} d\tau \frac{h(\tau) \sinh^2(\tau)}{\sqrt{1 - \left(\frac{\sinh \tau_0}{\sinh \tau}\right)^2 \left(\frac{\sinh(2\tau_0) - 2\tau_0}{\sinh(2\tau) - 2\tau}\right)^{\frac{2}{3}}}}. \quad (3.36)$$

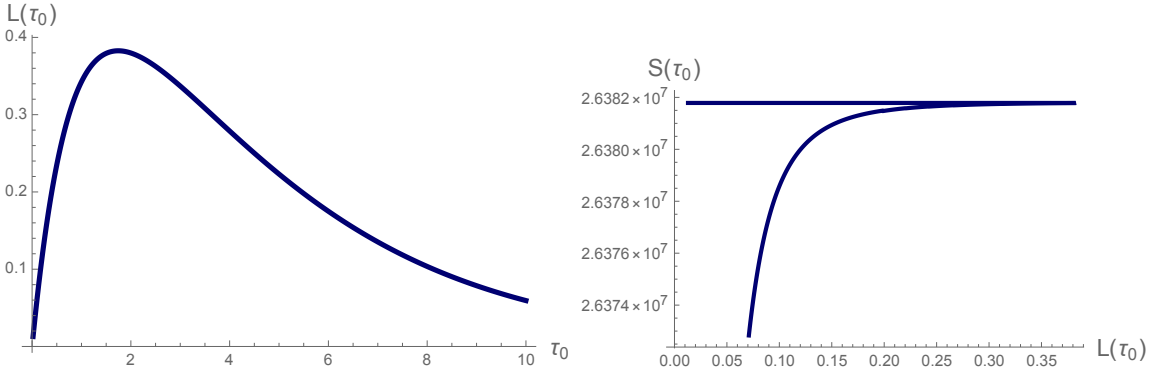


Figure 20. The relationship between width of a strip versus turning point τ_0 (in the left), and entanglement entropy versus L (in the right) in Klebanov-Strassler background.

The determinant of the eight-dimensional matrix which is needed would be found as

$$\det(\gamma_{ab}) = \frac{h^4 \epsilon^8}{9216} \sin^2 \theta_1 \sin^2 \theta_2 \left(\cos^2 \psi - \cosh^2 \left(\frac{\tau}{2}\right) \cosh \tau\right) \left(\cos^2 \psi - \cosh^2 \tau\right), \quad (3.37)$$

so we get

$$\Gamma_{\text{KS}} = \frac{\epsilon^8}{9216} \int_0^{2\pi} d\theta_1 \int_0^{2\pi} d\theta_2 \int_0^{2\pi} d\psi \int_{\tau_D}^{\tau_{2l+D}} d\tau h^4(\tau) \left(\cos^2 \psi - \cosh^2 \left(\frac{\tau}{2}\right) \cosh \tau\right) \left(\cos^2 \psi - \cosh^2 \tau\right). \quad (3.38)$$

The parameter M , α' or g_s could be changed which correspondingly change $h(\tau)$, and therefore the behavior of the critical D in this background can be studied which probes the phase structures.

Generally, the behavior of D_c versus the width of the two symmetric strips l in the Klebanov-Strassler background would be as shown in figure 21.

It could be seen that for small width of the strips the critical distance would increase by increasing l , but after reaching to a maximum it would decrease at then becomes constant.

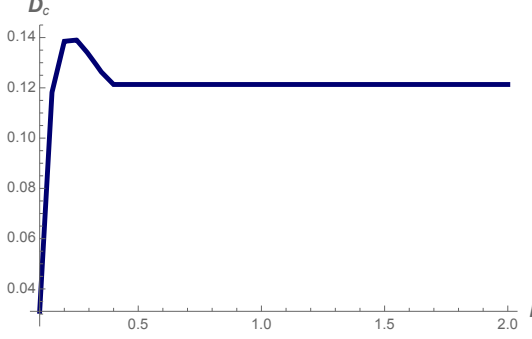


Figure 21. The behavior of critical distance, D_c , between the two strips in mixed systems, in the Klebanov-Strassler background.

3.5 Klebanov-Tseytin

The Klebanov-Tseytin (KT) metric is a singular solution which is dual to the chirally symmetric phase of the Klebanov-Strassler model which has D3-brane charges that dissolve in the flux [30].

The metric is

$$ds_{10}^2 = h(r)^{-1/2} [-dt^2 + d\vec{x}^2] + h(r)^{1/2} [dr^2 + r^2 ds_{T^{1,1}}^2]. \quad (3.39)$$

Here $ds_{T^{1,1}}^2$ is a base of a cone with the definition of

$$ds_{T^{1,1}}^2 = \frac{1}{9}(g^5)^2 + \frac{1}{6} \sum_{i=1}^4 (g^i)^2. \quad (3.40)$$

It is actually the metric on the coset space $T^{1,1} = (SU(2) \times SU(2))/U(1)$.

Also, g^i are some functions of the angles $\theta_1, \theta_2, \phi_1, \phi_2, \psi$ as

$$\begin{aligned} g^1 &= (-\sin \theta_1 d\phi_1 - \cos \psi \sin \theta_2 d\phi_2 + \sin \psi d\theta_2)/\sqrt{2}, & g^2 &= (d\theta_1 - \sin \psi \sin \theta_2 d\phi_2 - \cos \psi d\theta_2)/\sqrt{2}, \\ g^3 &= (-\sin \theta_1 d\phi_1 + \cos \psi \sin \theta_2 d\phi_2 - \sin \psi d\theta_2)\sqrt{2}, & g^4 &= (d\theta_1 + \sin \psi \sin \theta_2 d\phi_2 + \cos \psi d\theta_2)/\sqrt{2}, \\ g^5 &= d\psi + \cos \theta_1 d\phi_1 + \cos \theta_2 d\phi_2, \end{aligned} \quad (3.41)$$

and also we have the relations

$$h(r) = \frac{L^4}{r^4} \ln \frac{r}{r_s}, \quad L^4 = \frac{81}{2} g_s M^2 \epsilon^4. \quad (3.42)$$

In this frame, the asymptotic flat region has been eliminated. Also, $r = r_s$ is where the naked singularity is located.

The width of one strip versus turning point of RT surface in KT background can be written as [23]

$$L(r_0) = 9\sqrt{2}M\sqrt{g_s}\epsilon^2 \int_{r_0}^{\infty} dr \frac{\sqrt{\ln \frac{r}{r_s}}}{r^2 \sqrt{\frac{r^6 \ln \frac{r}{r_s}}{r_0^6 \ln \frac{r_0}{r_s}} - 1}}, \quad (3.43)$$

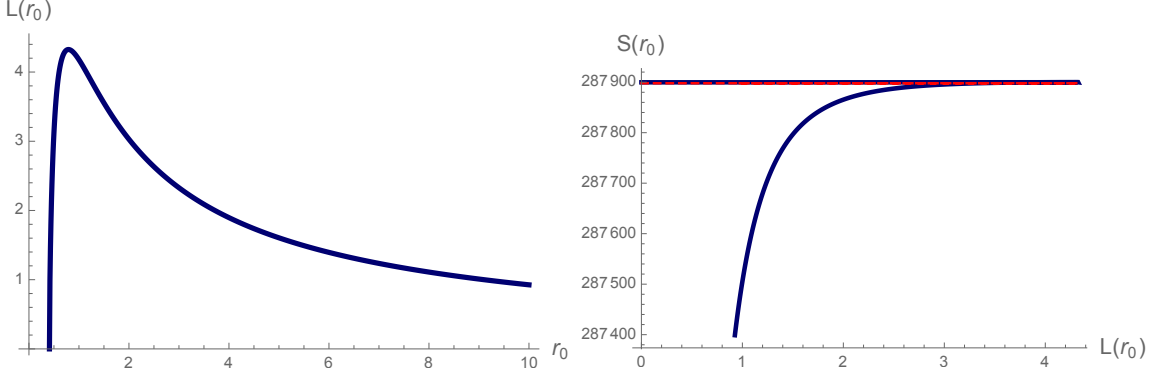


Figure 22. The relationship between width of a strip $L(r_0)$ versus turning point r_0 (in the left), and entanglement entropy $S(r_0)$ versus L (in the right) in the Klebanov-Tseytlin background.

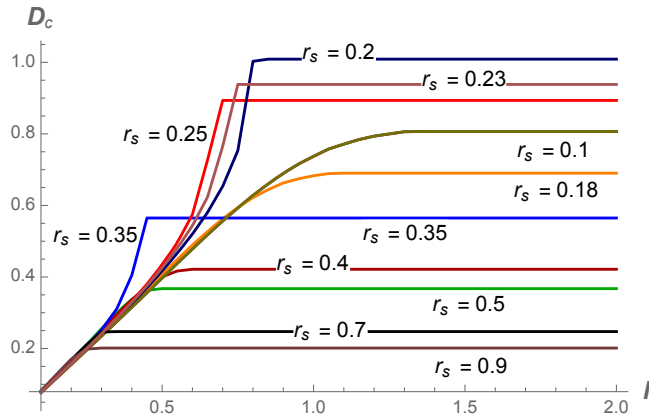


Figure 23. The relationship between the critical distance D_c between the two strips versus l in the Klebanov-Tseytlin geometry. The regions below each curve for each r_s correspond to non-zero mutual information and r_s corresponds to the position of the singularity.

and the entanglement entropy of the connected solution is

$$S_C(r_0) = \frac{12V_2\pi^3 M^2 g_s \epsilon^4}{G_N^{(10)}} \int_{r_0}^{\infty} dr \frac{r \ln \frac{r}{r_s}}{\sqrt{1 - \frac{r_0^6 \ln \frac{r_0}{r_s}}{r^6 \ln \frac{r}{r_s}}}}, \quad (3.44)$$

where their behavior is shown in figure 22.

The determinant of the induced metric for calculating Γ would be

$$\gamma_{ab} = -\frac{h^4 r^{10} \sin^2(\theta_1)}{69984} \left(\cos(2\theta_1) + 2 \cos(2\theta_2) - 3 \right), \quad (3.45)$$

so we get

$$\Gamma_{KT} = \frac{1}{108\sqrt{6}} \int_{r_D}^{r_{2l+D}} dr h^2(r) r^5 \int_0^{2\pi} \int_0^{2\pi} d\theta_1 d\theta_2 \sqrt{-3 + \cos 2\theta_1 + 2 \cos 2\theta_2} \sin \theta_1. \quad (3.46)$$

The phase structure coming from changing r_s is presented in figure 23. From figure 23, it could be seen that the relation of critical distance between the two strip versus l is

not a monotonic function in all the phase space, and again, by studying the behavior of D_c and therefore EoP, at least four different phases could be detected in these top-down QCD models, and again this is consistent with the result of [14].

Note that again the numerics are very sensitive to the parameter r_s which is the position of naked singularity here, specially for smaller value of r_s .

3.6 Klebanov-Witten

The Klebanov-Witten solution is similar to the KT throat geometry but with no logarithmic warping [31]. Unlike the other four mentioned metrics, it is just a conformal geometry. We study this background to compare our previous results in confining cases with the conformal one.

The metric is

$$ds^2 = h^{-\frac{1}{2}} g_{\mu\nu} dx^\mu dx^\nu + h^{\frac{1}{2}} (dr^2 + r^2 ds_{T^{1,1}}^2), \quad (3.47)$$

where

$$h = \frac{L^4}{r^4}, \quad \text{and} \quad L^4 = \frac{27\pi}{4} g_s N(\alpha')^2. \quad (3.48)$$

Since the Klebanov-Witten solution is very similar to Klebanov-Tseytlin, the functional for calculating Γ would be similar, and only the relation for h is different, as it has no Logarithmic term.

$$\Gamma_{\text{KW}} = \frac{1}{108\sqrt{6}} \int_{r_D}^{r_{2l+D}} dr h^2(r) r^5 \int_0^{2\pi} \int_0^{2\pi} d\theta_1 d\theta_2 \sqrt{-3 + \cos 2\theta_1 + 2 \cos 2\theta_2} \sin \theta_1. \quad (3.49)$$

The width of the strip in terms of the turning point and the entanglement entropy could be written as

$$L(r_0) = 2L^2 \int_{r_0}^{\infty} dr \frac{1}{r^2 \sqrt{\frac{r^6}{r_0^6} - 1}}, \quad (3.50)$$

and

$$S(r_0) = \frac{8V_{d-1}\pi^4 L}{27G_N^{(10)}} \int_{r_0}^{\infty} dr \frac{r}{\sqrt{1 - \frac{r_0^6}{r^6}}}. \quad (3.51)$$

where their behavior is shown in figure 24.

The behavior of D_c versus l is shown in figure 25. Since this geometry is conformal and there is no position of the wall here, as in r_s , no rich phase structure could be detected, but the behavior of D_c is similar to the first phase of Klebanov-Tseytlin shown in figure 23, as one expects.

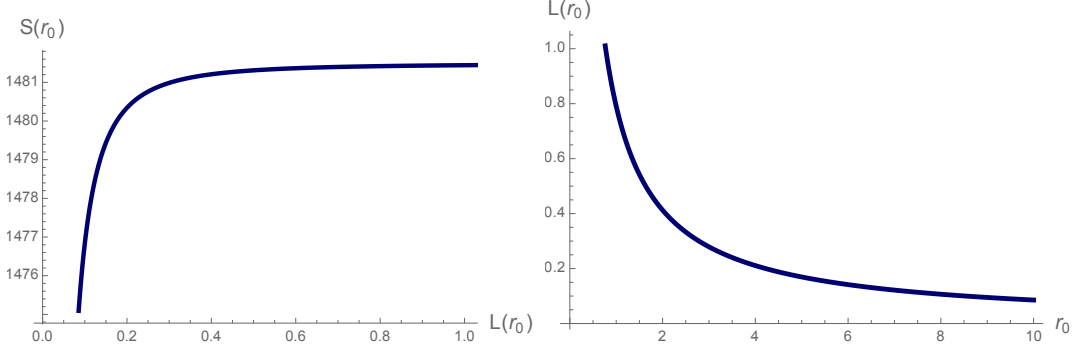


Figure 24. The relationship between width of a strip versus turning point r_0 (in the left), and entanglement entropy versus L (in the right) in the Klebanov-Witten (KW) background which shows similar behavior to AdS case.

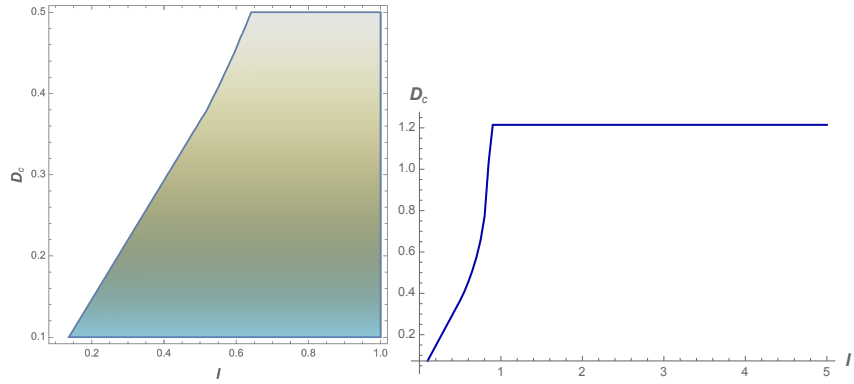


Figure 25. The behavior of D_c versus l in KW background in the right part and non-zero region of mutual information in the left.

3.7 Maldacena-Nunez

The Maldacena-Nunez (MN) metric is obtained by a large number of D5-branes wrapping on S^2 [32]. In the string frame the metric and the fields are written as [29]

$$ds_{10}^2 = e^\phi [-dt^2 + dx_1^2 + dx_2^2 + dx_3^2 + e^{2h(r)}(d\theta_1^2 + \sin^2 \theta_1 d\phi_1^2) + dr^2 + \frac{1}{4}(w^i - A^i)^2], \quad (3.52)$$

where

$$A^1 = -a(r)d\theta_1, \quad A^2 = a(r)\sin \theta_1 d\phi_1, \quad A^3 = -\cos \theta_1 d\phi_1, \quad (3.53)$$

and the ω^i 's parametrize the 3-sphere compactification, which are

$$\begin{aligned} w^1 &= \cos \psi d\theta_2 + \sin \psi \sin \theta_2 d\phi_2, & w^2 &= -\sin \psi d\theta_2 + \cos \psi \sin \theta_2 d\phi_2, \\ w^3 &= d\psi + \cos \theta_2 d\phi_2, \end{aligned} \quad (3.54)$$

and also the other parameters of the metric would be

$$a(r) = \frac{2r}{\sinh 2r}, \quad e^{2h} = r \coth 2r - \frac{r^2}{\sinh 2r^2} - \frac{1}{4}, \quad e^{-2\phi} = e^{-2\phi_0} \frac{2e^h}{\sinh 2r}. \quad (3.55)$$

The width of the strip versus turning point can be written as

$$L(r_0) = \int_{r_0}^{\infty} dr \frac{2}{\sqrt{\frac{\sinh^4(2r)}{\sinh^4(2r_0)} - 1}}, \quad (3.56)$$

and the entanglement entropy of the connected solution of the strip is

$$S_C(r_0) = \frac{V_2 \pi^3 e^{4\phi_0}}{G_N^{(10)}} \int_{r_0}^{\infty} dr \frac{\sinh^2(2r)}{\sqrt{1 - \frac{\sinh^4(2r_0)}{\sinh^4(2r)}}}. \quad (3.57)$$

The behavior of $L(r_0)$ and S are shown in figure 26.

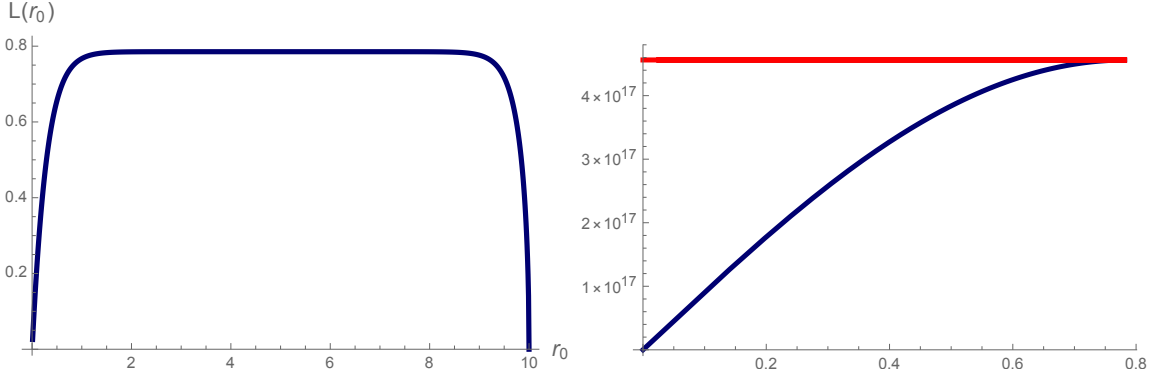


Figure 26. The relationship between width of a strip versus turning point r_0 (in the left), and entanglement entropy versus L (in the right) in the Maldacena-Nunez background.

The behavior of the critical distance versus L (one strip) is then shown in figure 27. Note that unlike other confining geometries, we don't have many free parameters in the MN case and therefore similar to the conformal case of KW, no phase structure could also be detected. The only difference here would be the early oscillations and noises in the behavior of D_c for small values of width, l , (for the case of two strips) which we have explained their origins in the confining backgrounds before.

Then, for this geometry, the determinant of the eight-dimensional induced metric for calculating Γ would be $\det \gamma_{ab} = e^{4h+8\phi} \sin^2(\theta_1) \sin^2(\theta_2)$, so after simplifications we get the following result for the minimal wedge cross section as

$$\Gamma_{MN} = \int_{r_D}^{r_{2l+D}} dr e^{4\phi_0} \cosh^2(r) \sinh^2(r). \quad (3.58)$$

where again the only free parameter are ϕ_0 or r_0 and no rich phase structure could be found here.

3.8 Domain Wall AdS/QCD

In the recent work [33, 34], using the domain wall structure, a new holographic model for QCD has been constructed which consists of probe D7 branes in a D5 brane geometry.

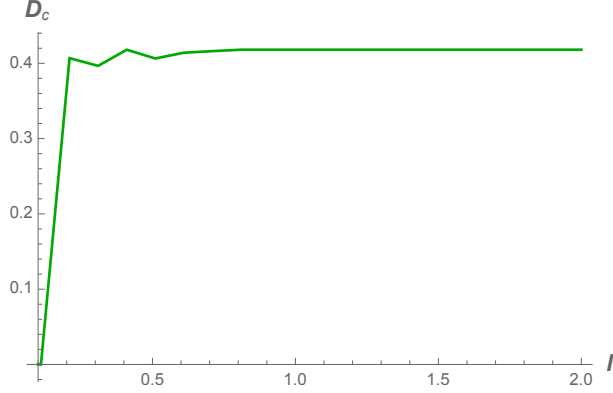


Figure 27. The relationship between width of a strip $L(r_0)$ versus turning point r_0 (in the left), and the entanglement entropy $S(L)$ versus L (in the right) in the Maldacena-Nunez background.

When one dimension of the D5 geometry is being compactified, the confinement will come into play and affects the gauge degrees of freedom in the theory.

The D5 geometry is

$$ds^2 = \frac{u}{R} (\eta_{\mu\nu} dx^\mu dx^\nu + dx_4^2 + dx_5^2 f(u; u_\Lambda)) + \frac{R}{u} \frac{du^2}{f(u; u_\Lambda)} + R u d\Omega_3^2, \quad (3.59)$$

where

$$f(u; u_\Lambda) = \left(1 - \frac{u_\Lambda^2}{u^2}\right), \quad (3.60)$$

and the non trivial dilaton field and 3-form flux are

$$e^\phi = g_s \frac{u}{R}, \quad F_3 = \frac{2R^2}{g_s} \Omega_3, \quad (3.61)$$

where Ω_3 is the volume form of the unit 3-sphere and the parameter R is related to the string parameters as $R^2 = g_s N_c \alpha'$.

The entanglement entropy as the function of turning point u_t could be found as

$$S_C(u_t) = \frac{(2\pi)^2 V_2 V_3}{2g_s^2 G_N^{(10)}} \int_{u_t}^{\infty} du \frac{u}{\sqrt{1 - \frac{u_t^4}{u^4} \left(\frac{1 - \frac{u_\Lambda^2}{u^2}}{1 - \frac{u_\Lambda^2}{u_t^2}} \right)}}, \quad (3.62)$$

and the width of the strip versus the turning point is

$$L(u_t) = 2R \int_{u_t}^{\infty} \frac{du}{u} \frac{1}{\sqrt{\left(1 - \frac{u_\Lambda^2}{u^2}\right) \left(\frac{u^4}{u_t^4} \frac{1 - \frac{u_\Lambda^2}{u^2}}{1 - \frac{u_\Lambda^2}{u_t^2}} - 1\right)}}. \quad (3.63)$$

Their behavior is shown in figure 28, where again the typical and universal behavior of the QCD models, as the butterfly geometry for S , can be detected.

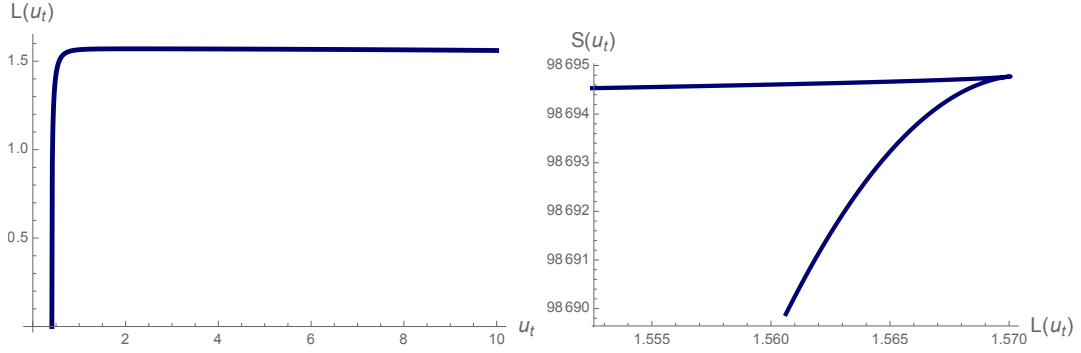


Figure 28. The behavior of $L(u_t)$ versus u_t and $S(u_t)$ versus $L(u_t)$ in the domain wall QCD.

Then, the critical distance D_c between the two strips versus their width l could be studied, where again different values of u_Λ can capture many interesting phase structures in this background, where the results are shown in figures 29, 30, and 31.

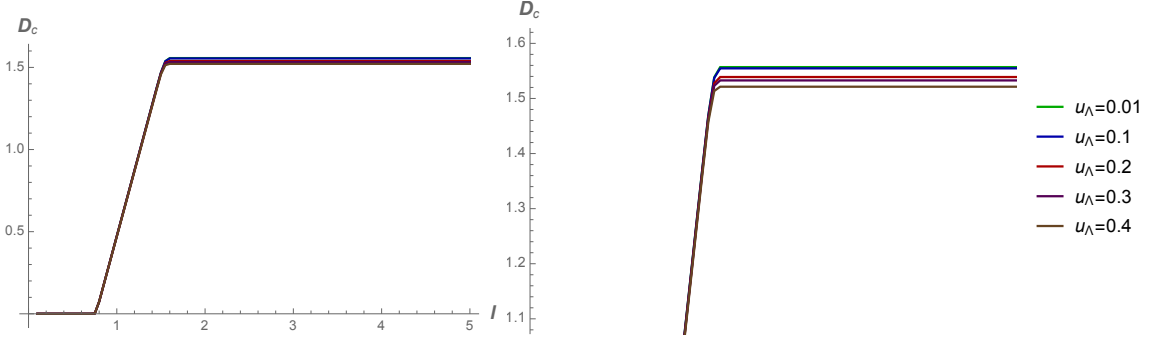


Figure 29. Phase one in D5 background.

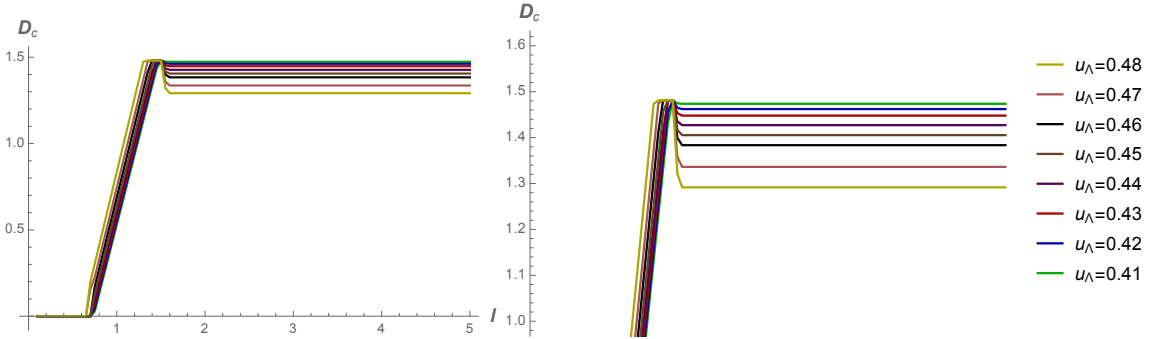


Figure 30. Phase two in D5 background.

Increasing u_Λ after 0.49 would make D_c negative which is not an acceptable range of parameter for this quantity, but still the behavior is shown in figure 31.

More phases can be detected by increasing u_Λ , but it would become more noisy.

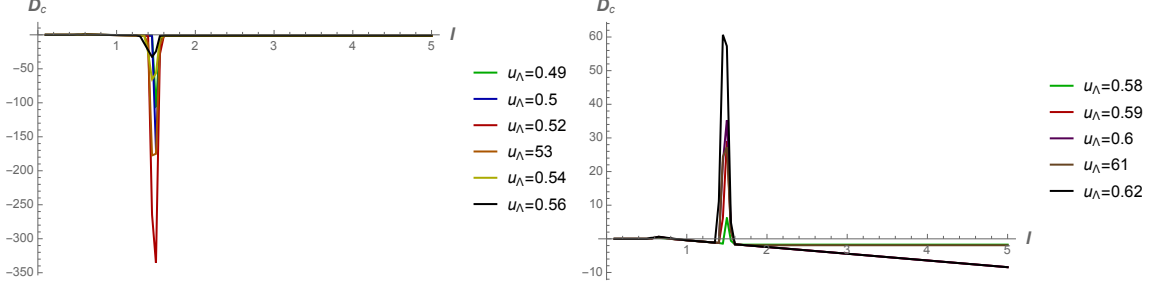


Figure 31. Phase three or the range of u_Λ which D_c is negative is shown in the left part, and the phase four is shown in the right part.

For this case, the results are less noisy but again some sharp jumps can be observed. The behavior of the quasi-normal modes would have significant effects on the quantum information measures in this case.

It would then be interesting to compare the behavior of quasi-normal modes (QNM) of D-branes, and the geodesic motions in each of these models as in [35] and check the connections between the quantum Sieberg-Witten (SW) curves and the gravitational perturbations dubbed SW-QNM correspondence. Specially, the behavior of QNMs around the phase transitions and the connections with the critical distance, mutual information, EoP and negativity could be studied.

Also, the calculations of mixed quantum measures could be done for the fully-localized D3/D7 intersection, where the branes are located at a fix location in the transverse direction. The results can also be compared with other backgrounds and also with the geometries where these branes are smeared.

Its metric would be

$$ds_{10}^2 = h^{-1/2} \eta_{\mu\nu} dx^\mu dx^\nu + h^{1/2} \left(d\rho^2 + \rho^2 d\Omega_3^2 + e^{-\phi} (d\omega^2 + \omega^2 d\theta^2) \right), \quad (3.64)$$

where here the (near-core) wrap factor $h = h(\rho, \omega)$ is

$$h(\rho, \omega) = 1 + \frac{R^4}{(\rho^2 + e^{-\phi} \omega^2)^2}, \quad (3.65)$$

where $R^4 = 4\pi g_s N \alpha'^2$ and the dilaton field ϕ and axion field χ can be found from the relations $e^{-\phi(\omega)} = \beta_0 \log \frac{\omega_\Lambda^2}{\omega}$ and $\chi(\theta) = \frac{N_f}{2\pi} \theta$, where the integration constants are $\beta_0 = \frac{N_f}{4\pi}$ and $\omega_\Lambda^2 = \omega_0^2 e^{1/(g_s \beta_0)}$.

The main difference about this geometry is that the factor $h(\rho, \omega)$ is a factor of both of the coordinates ρ and ω which makes the calculations more difficult and we leave it for the future works. Note that, for the small values of ω , the near-core region of D3/D7 intersection corresponds to the IR region of the dual field theory. This background contains RR four-form potential of the D3-brane solution which then its effects on the correlations between the two mixed strips could be studied.

Note that for constructing these results we just used the connected part of the entanglement entropy, i.e., S_C . We could also use the regularized entropy, $S_C - S_D$, where S_D is

the solution for the “disconnected part” which is just a constant, and then in the numerical codes we could take the minimum of S_C and S_D . For example for the Witten-QCD case, we could get somehow a different phase diagram as shown in figure 32. But the general results would be similar and no more phases can be detected using this quantity instead of S_C .

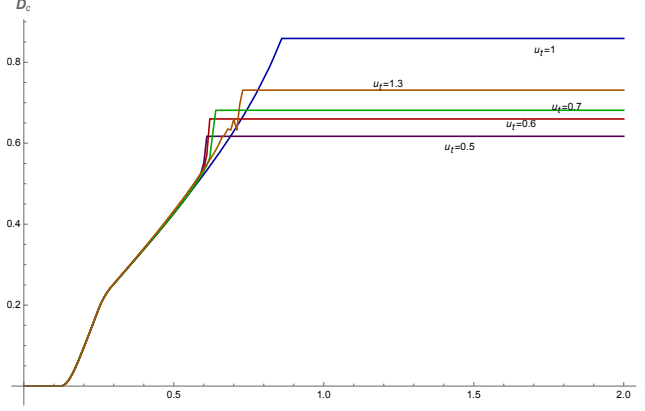


Figure 32. The phase diagram for calculating D_c , coming from $S_C - S_D$.

4 Crofton form in confining backgrounds

For checking the interconnections between geometry and topology, and the quantum information measures, it would be interesting to calculate the Crofton form for these confining models as well and compare its behaviors for each case.

In [12], using ideas from integral geometry, the authors found the connections between the length of a curve and the number of geodesics, or “random” lines it would be intersected and therefore its connection to the Crofton formula. This formula can give further intuitions about the structures of these various confining backgrounds from the perspective of the bulk reconstruction and can shed more lights on their various specific properties such as singularities, throats, bulges, walls, etc and their effects on the correlations between the two strips in the mixed setup in such confining models. Therefore, the behavior of the Crofton form for each space will be presented here.

4.1 AdS-soliton

The Crofton form for the AdS-soliton geometry with the metric 3.2 would be

$$\omega_{\text{AdS-soliton}} = \frac{\left(2z_0 - \frac{(d-6)z^8\left(\frac{z}{z_0}\right)^{-d}}{z_0^7}\right)\left(1 - \left(\frac{z_t}{z_0}\right)^{8-d}\right)}{2z_0z_t^2\left(1 - \left(\frac{z}{z_0}\right)^{8-d}\right)^2\left(1 - \frac{z^2\left(1 - \left(\frac{z_t}{z_0}\right)^{8-d}\right)}{\left(1 - \left(\frac{z}{z_0}\right)^{8-d}\right)z_t^2}\right)^{\frac{3}{2}}} - \frac{1}{z^2\sqrt{1 - \frac{z^2\left(1 - \left(\frac{z_t}{z_0}\right)^{8-d}\right)}{\left(1 - \left(\frac{z}{z_0}\right)^{8-d}\right)^2z_t}}}, \quad (4.1)$$

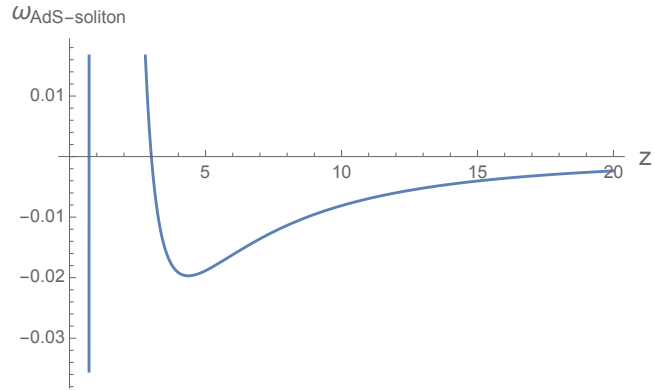


Figure 33. The plot of Crofton form ω vs. z in AdS-soliton background.

which its behavior is shown in figure 33.

If one uses other forms of metric for AdS soliton, for instance the form of metric of 3.7, one could get plots with a general similar behavior as shown in figures 34 or 35.

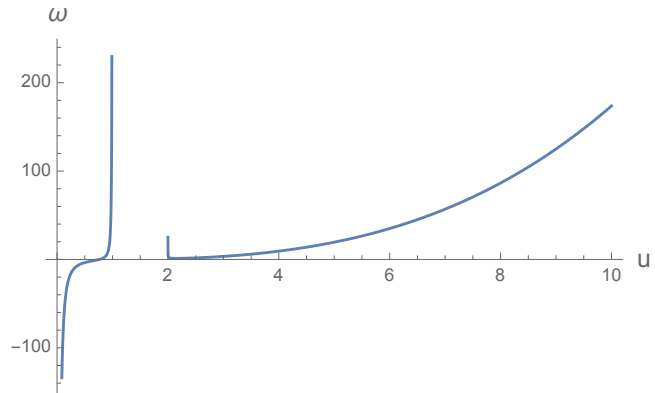


Figure 34. The plot of Crofton form ω vs. z in AdS-soliton background.

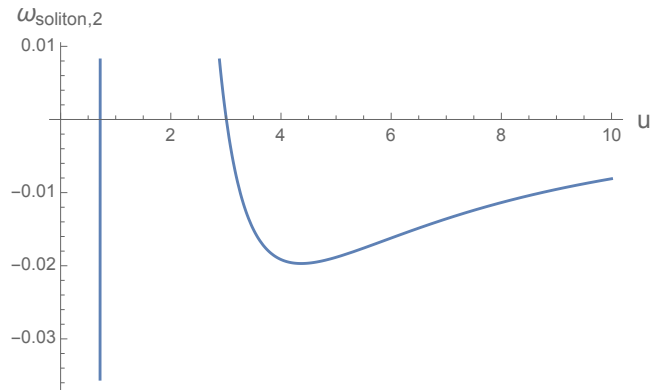


Figure 35. The plot of Crofton form ω vs. z in AdS-soliton background.

So one could see that the standard behavior is similar, excepts for some constants, as a well is being formed around the singularity, or the turning points, while in the larger AdS-radius, ω increases, with also a decreasing gradient, or as we see later, it would become constant for $u \rightarrow \infty$.

Note that a similar quantity to Crofton form could also be defined by $\frac{\partial^2 S}{\partial L^2}$ as well, which after L_{crit} it becomes zero and before that, it is the second derivative of the green curve of figure 36, and for large values of u , it becomes constant. This new quantity could also give further information.

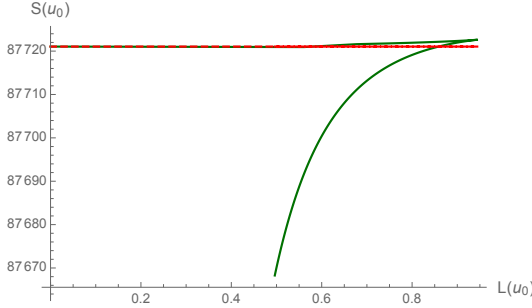


Figure 36. The general behavior S vs. L in confining models. The second derivative of the green curve (versus L instead of u) could be used to define a new quantity similar to the Crofton form which could give further information about the interplay between geometry and information.

4.2 Sakai-Sugimoto and deformed Sakai-Sugimoto

The Crofton form of Sakai-Sugimoto geometry would be

$$\omega_{\text{Sakai-Sugimoto}} = \frac{V_3 V_4 R_{D_4}^3}{2g_s^2 G_N^{(10)}} \frac{u^4 (10u_{\text{KK}}^3 u_t^5 - 5u^5 u_{\text{KK}}^3 - 7u^3 u_t^5 + 2u^8)}{2((u^3 - u_{\text{KK}}^3)(u^5 - u_t^5))^{\frac{3}{2}}} du \wedge d\theta. \quad (4.2)$$

The plot of Crofton form ω versus u for $u_{\text{KK}} = 1$ and $u_t = 2$ has been shown in figure 37. One can again detect a well around u_t and it becomes constant in the large values of u .

For the deformed case we get two additional term as

$$\begin{aligned} \omega_{\text{deformed Sakai-Sugimoto}} = & \frac{V_3 V_4 R_{D_4}^3}{2g_s^2 G_N^{(10)}} \left[\frac{u^4 (10u_{\text{KK}}^3 u_t^5 - 5u^5 u_{\text{KK}}^3 - 7u^3 u_t^5 + 2u^8)}{2((u^3 - u_{\text{KK}}^3)(u^5 - u_t^5))^{\frac{3}{2}}} \right. \\ & + \frac{d^2 x^4(u)}{du^2} \sqrt{\frac{u^5 (1 - \frac{u_{\text{KK}}^3}{u^3})}{1 - \frac{u_t^5}{u^5}}} \\ & \left. + \frac{dx^4(u)}{du} \frac{u^{5/2} (7u_{\text{KK}}^3 u_t^5 - 2u^5 u_{\text{KK}}^3 - 10u^3 u_t^5 + 5u^8)}{2((u^3 - u_{\text{KK}}^3)(u^5 - u_t^5))^{\frac{3}{2}}} \right] du \wedge d\theta, \end{aligned}$$

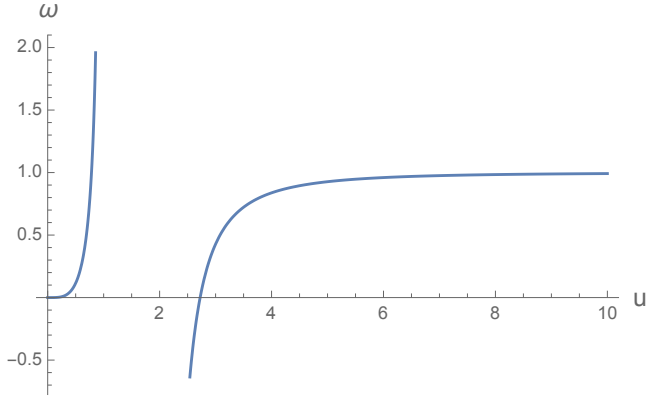


Figure 37. The plot of Crofton form ω vs. r in the Sakai-Sugimoto background.

Then, using the relation 3.22, we get

$$\begin{aligned} \omega_{\text{deformed Sakai-Sugimoto}} = & \frac{V_3 V_4 R_{D_4}^3}{2 g_s^2 G_N^{(10)}} \frac{u^4}{2 \left(\frac{u^8 - u^5 u_{\text{KK}}^3}{u_0^8 - u_0^5 u_{\text{KK}}^3} - 1 \right)^{\frac{1}{2}} (u^3 - u_{\text{KK}}^3)^{\frac{3}{2}} (u^5 - u_t)^{\frac{3}{2}}} \times \\ & \left(\frac{R_{D_4}^{\frac{3}{2}} (3u_0^8 u^3 - (2u^5 + 3u_0^5) u_{\text{KK}}^6 + (13u^8 - 3u_0^5 u^3 + 3u_0^8) u_{\text{KK}}^3 - 11u^{11}) (u^5 - u_t^5)}{u_0^5 u_{\text{KK}}^3 - u^5 u_{\text{KK}}^3 + u^8 - u_0^8} \right. \\ & + R_{D_4}^{\frac{3}{2}} (7u_{\text{KK}}^3 u_t^5 - 2u^5 u_{\text{KK}}^3 - 10u^3 u_t^5 + 5u^8) \\ & \left. + \left(\frac{u^8 - u^5 u_{\text{KK}}^3}{u_0^8 - u_0^5 u_{\text{KK}}^3} - 1 \right)^{\frac{1}{2}} (10u_{\text{KK}}^3 u_t^5 - 5u^5 u_{\text{KK}}^3 - 7u^3 u_t^5 + 2u^8) \right) du \wedge d\theta, \end{aligned}$$

The general behavior of $\omega_{\text{deformed Sakai-Sugimoto}}$ vs. u is shown in figure 38.

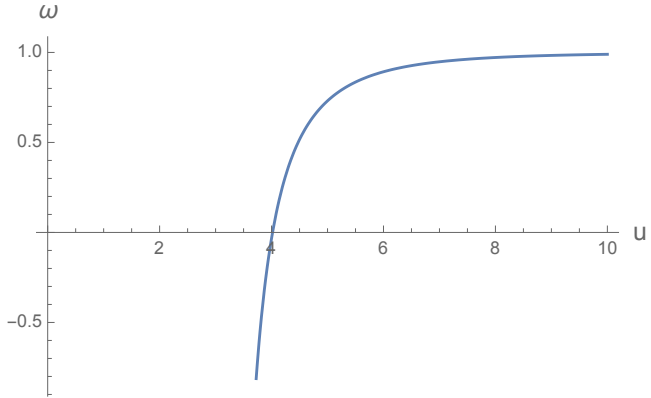


Figure 38. The plot of Crofton form ω vs. r in the *deformed Sakai-Sugimoto background*.

One could see that for the intermediate and bigger values of u the behavior is similar to the Sakai-Sugimoto case, as one would expect.

4.3 Klebanov-Strassler

The Crofton form in the KS background would be

$$\omega_{\text{KS}} = \frac{2^{2/3} \pi^3 V_2 \epsilon^{-8/3} \epsilon^4 (\alpha_p g_s M)^2}{3G_N} \frac{h(\tau) \sinh(2\tau)}{\sqrt{1 - \sinh^2(\tau_0) \cosh^2(\tau) \left(\frac{\tau_0 - \sinh(\tau_0) \cosh(\tau_0)}{\tau - \sinh(\tau) \cosh(\tau)}\right)^{\frac{2}{3}}}} -$$

$$\frac{h(\tau) \sinh^2(\tau_0) (2\tau_0 - \sinh(2\tau_0)) (12\tau \coth(\tau) - 5 \sinh(3\tau) \cosh(\tau) + 3)}{6(\sinh(2\tau) - 2\tau)^2 \sqrt[3]{\frac{\tau_0 - \sinh(\tau_0) \cosh(\tau_0)}{\tau - \sinh(\tau) \cosh(\tau)}} \left(1 - \sinh^2(\tau_0) \cosh^2(\tau) \left(\frac{\tau_0 - \sinh(\tau_0) \cosh(\tau_0)}{\tau - \sinh(\tau) \cosh(\tau)}\right)^{\frac{2}{3}}\right)^{\frac{3}{2}}} +$$

$$\frac{\sinh^2(\tau) h'(\tau)}{\sqrt{1 - \sinh^2(\tau_0) \cosh^2(\tau) \left(\frac{\tau_0 - \sinh(\tau_0) \cosh(\tau_0)}{\tau - \sinh(\tau) \cosh(\tau)}\right)^{\frac{2}{3}}}}.$$

Due to the integral in the relation of $h(\tau)$ function, the analytic solution could not be found and the Crofton form for the KS could only be studied numerically. We expect its behavior would be very similar to the KT case, as in figure 41.

4.4 Witten-QCD

The Crofton form for the Witten-QCD model is

$$\omega = \frac{-1}{2} \partial_u^2 S du \wedge d\theta =$$

$$\frac{V_2}{G_N^{(10)}} \frac{4\pi^2 R^{\frac{9}{2}}}{9g_s^2 \sqrt{u_t}} \left(\frac{u (2(u^2 - 2u_0^2) u_t^6 + (7u_0^2 u^3 + 4u_0^5 - 4u^5) u_t^3 + 2u^8 - 7u_0^5 u^3)}{2(u^5 - u_0^5 - u^2(u_t^3 - u_0^2))^{\frac{3}{2}} \sqrt{u^3 - u_t^3}} \right) du \wedge d\theta.$$

Note that again we only use the connected solution for entanglement entropy here.

The behavior of Crofton form for $u_0 = 2$ and $u_t = 1$ in WQCD background has been shown in figure 39 where one can see that around u_t and u_0 we have an infinite well.

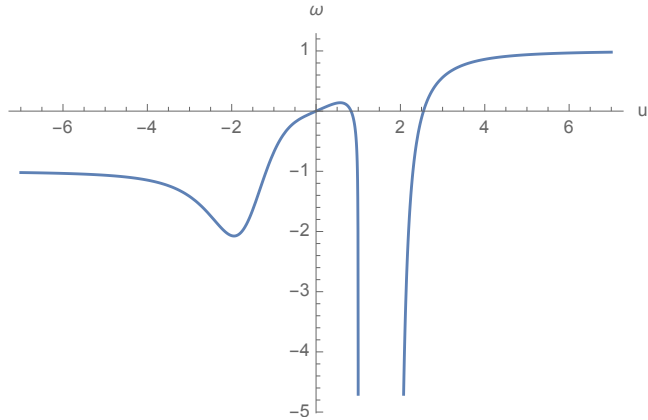


Figure 39. The plot of Crofton form ω vs. u in WQCD background.

4.5 Maldacena-Nunez

The Crofton form in MN background would be

$$\omega_{MN} = c_{MN} \frac{2 \sinh(4r) (\sinh^4(2r) - 2 \sinh^4(2r_0))}{(\sinh^4(2r) - \sinh^4(2r_0)) \sqrt{1 - \sinh^4(2r_0) \cosh^4(2r)}}, \quad (4.3)$$

where $c_{MN} = \frac{V_2 \pi^3 e^{4\phi_0}}{G_N^{(10)}}$.

The plot of Crofton form for $r_0 = 2$ in MN case has been shown in figure 40. Again a deep well could be detected.

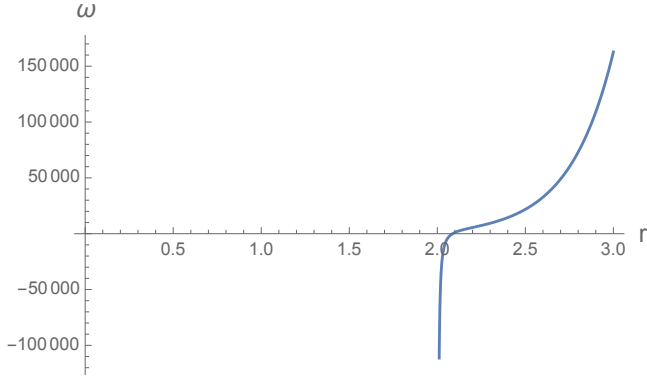


Figure 40. The plot of Crofton form ω vs. r in the MN background.

4.6 Klebanov-Tseytlin

The Crofton form for the KT background would be

$$\omega_{KT} = c_{KT} \frac{2r^9 \log^{\frac{3}{2}}\left(\frac{r}{r_s}\right) \left(\log\left(\frac{r}{r_s}\right) + 1\right) - r_0^6 r^3 \log\left(\frac{r_0}{r_s}\right) \log^{\frac{1}{2}}\left(\frac{r}{r_s}\right) \left(8 \log\left(\frac{r}{r_s}\right) + 3\right)}{2 \left(r^6 \log\left(\frac{r}{r_s}\right) - r_0^6 \log\left(\frac{r_0}{r_s}\right)\right)^{\frac{3}{2}}}, \quad (4.4)$$

where $c_{KT} = \frac{12V_2 \pi^3 M^2 g_s \epsilon^4}{G_N^{(10)}}$ is just a constant.

The plot of ω_{KT} versus r for singularity point of $r_s = 2$ and turning point of $r_0 = 1$ is shown in figure 41.

Again, one can see similar to the WQCD case, for the Crofton form, there is a well around the singularity point.

4.7 Domain Wall QCD

The Crofton form for the D5 black brane 3.59 which were used in the domain wall background 3.8 is

$$\omega = \frac{u (u^2 (3u_t^2 u_\Lambda^2 - 3u_t^4 + u_\Lambda^4) + 2u_t^2 u_\Lambda^2 (u_t^2 - u_\Lambda^2) + u^6 - 2u^4 u_\Lambda^2)}{(u^2 - u_\Lambda^2)^{\frac{1}{2}} ((u^2 - u_t^2) (u_t^2 + u^2 - u_\Lambda^2))^{\frac{3}{2}}} \quad (4.5)$$

Again, the hole around the u_Λ and u_t could be detected while for the larger values of u it would become constant and again it would point to the structure of this background as the Crofton form can be used as a holographic tool in the bulk reconstruction.

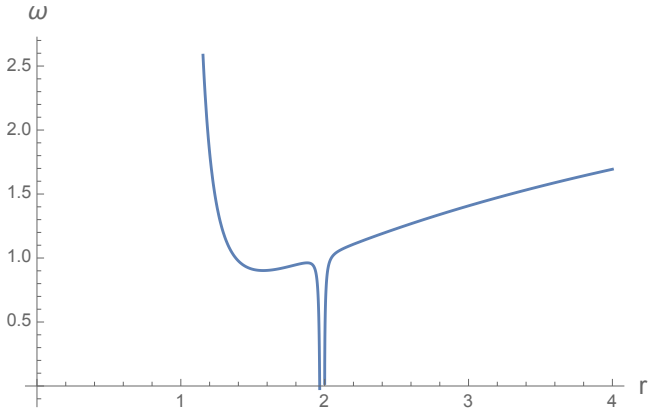


Figure 41. The plot of Crofton form ω vs. r in the KT background.

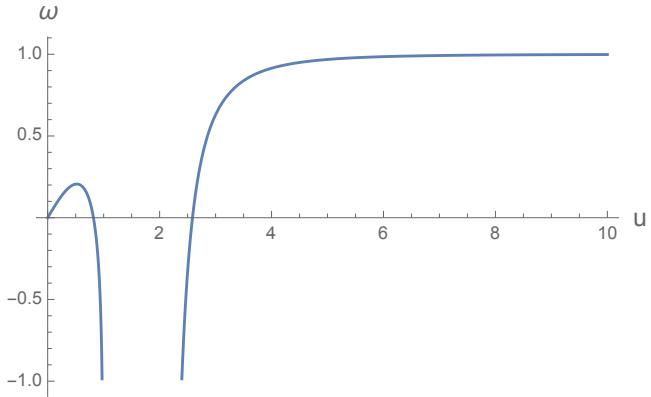


Figure 42. The Crofton form for D5 black brane geometry for $u_t = 2$ and $u_\Lambda = 1$.

5 Other holographic quantum measures in probing QCD phases

In this section, we briefly discuss other holographic tools and quantum measures which could also probe the confining geometries and detect the phase transitions and structures of the complex holographic QCD models.

5.1 Quantum negativity in confining backgrounds

First, the entanglement wedge has been studied in [9] and using the geometrical perspective, another quantity dubbed complexity of purification and its bulk holographic dual, and also its connection with the minimal wedge cross section and EoP have been discussed. As this quantity is a volume and probe more space in the bulk and could go deep in the bulk, we expect that it could also gain many properties of the rich structures of QCD.

Also, in quantum many body systems, a new quantum measure called negativity $\mathcal{N}(\rho) = \frac{\|\rho^F\|_1 - 1}{2}$, and the logarithmic negativity $\epsilon(\rho) = \log \|\rho^F\|_1$, have been introduced, where the sign $\|\mathcal{O}\|_1$ is actually the trace-norm of the operator, i.e, $\|\mathcal{O}\|_1 = \text{Tr}(\sqrt{\mathcal{O}^\dagger \mathcal{O}})$.

Using its holographic dual prescription, in [14], for three confining backgrounds, the entanglement negativity as the combination of various extremal surface has been calculated and then it has been used to construct their phase diagrams. The authors used the relation [14, 36]

$$\mathcal{N} = \frac{3}{4} (2S(l+D) - S(2l+D) - S(D)), \quad (5.1)$$

which again is for two symmetric, parallel strips with width l and distance D between them.

This could also easily be calculated in our specific confining backgrounds, and the phase diagrams using this quantity then be probed. We expect that, by using the quantity D_{crit} , negativity could also distinguish the scale for confinement/deconfinement versus chiral symmetry breaking, specially in backgrounds such as Saka-Sugimoto and Klebanov-Tseytlin, as we have observed here. This is because specifically in these two backgrounds, it is possible to change the position of singularity, i.e, r_s and the phases would be distinguished more clearly.

5.2 Calibrated geometry and bit threads in confining geometries

In order to find the entanglement entropy of a region with its complement, from the convex optimization theory, the problem of minimizing surfaces which are homologous to a boundary region A , could be recast to the problem of maximizing the number of bit threads that connect A to its complement and satisfy the following norm bound

$$S(A) = \max_{v^\mu} \int_A \sqrt{h} n_\mu v^\mu, \text{ s.t. } \nabla_\mu v^\mu = 0, |v^\mu| \leq 1, \quad (5.2)$$

where \sqrt{h} is the induced metric on the boundary and n^μ is the unit normal.

So the generalized calibrated geometry, [37–40] would have interesting connections to bit thread formalism and max-flow, min-cut theorem, and also to recent quantum bit threads proposal [28]. These then could be employed in the confining models as well and one can check whether these tools could also capture the phase transitions and distinguish the scale of confinement/deconfinement versus other physical scales in the theory such as chiral symmetry breaking/restoration. In fact, in a recent work [41, 42], the notion of Lorentzian bit thread flow for the construction of complexity (volume) and emergence of time has been introduced. These studies could show the ability of these mathematical tools to probe such singularities in the bulk, and the physical scales in the boundary.

In a recent work, [43], the connections between balanced partial entanglement and the entanglement wedge cross section has been studied and then in [44], for the holographic entanglement contours, the quantum corrections and also its first thermodynamic law has been investigated. So another interesting path is to study the pattern of entanglement using other measures such as balanced partial entanglement [43], entanglement contours [44], horocycles [45], lambda lengths of Penner [46]. Also works similar to [47] could be repeated for confining geometries, as their study has been done for the case of BTZ black hole where in that case they showed that the entanglement pattern would follow a C_{N-1} cluster algebra.

So this could be repeated for our confining geometry cases and their behavior for each case could be examined. The behavior of partitions of states, mutations and flips then could also be studied in the confining field theories. For doing this study, as the first step, we could use the result of calculations of Kinematic space for each of these geometries which have been performed in section 4. Additionally, the new quantities of *partial transpose* (*PT*) and the “*spectrum of negativity*” as other measures of correlations between mixed states could also be used to probe the topologies of confining geometries and the phase structures of QCD.

In addition, the modular Hamiltonian and modular flow structure for the confining/AdS soliton case could also be calculated which is the purpose of our future works.

In a recent work [48], the shape of contours of entanglement islands in two dimensional boundary field theories (BCFTs) has been worked out. Note that these entanglement contours are spatially and quasilocal extension of entanglement entropy. Specifically in [48], they have found that the boundary can induce discontinuities in the contours. We expect that these discontinuities would also be observed in the confining cases, for instance in the end-point of AdS-soliton case, which could also reveal the hidden localization-delocalization patterns of the entanglement degrees of freedom in these confining geometries. The form of the Page curve for confining geometries could also be investigated. So it would be interesting to re-evaluate our results in the setup of island formulations.

Another interesting quantity would be the “Holevo information” which is being defined as

$$\chi(\rho, \rho_i, p_i) \equiv S(\rho) - \sum_i p_i S(\rho_i), \quad (5.3)$$

and has been used in [49] to study the black hole mesostates and also to detect the phase transitions in the bulk wormholes geometry which contain black holes with different horizon sizes. It could also be calculated in the confining backgrounds and its connections to mixed correlation, EoP or bit threads could then be studied.

Another interesting recent work [50] which depicts the scalar fields as the $N \times N$ matrices with color indices, which would lead to the transverse spatial direction in the bulk could also be used in our studies of constructing QCD phases using quantum information measures. In their work, the bulk space-time would emerge from the color degrees of freedom in the boundary-Yang-Mills theory. So the question would be how various color degrees of freedom in various models of QCD would change the specific geometric structures, modular Hamiltonian, or how it correspondingly change the eigenvalues of the locations of D-branes which then lead to the emergence of various bulk dual geometries like Klebanov-Strassler with its exotic throat, Witten QCD, AdS soliton models, etc.

In [51], it has been shown that the gradient flow of gauge fields and the smearing procedure could act as a neural network. The role of the projection in the smearing function and bulk reconstruction procedure has been pointed out. For instance by applying the gradient flow to non-linear sigma model, the AdS geometry could be reconstructed. These studies could also be repeated for our backgrounds.

Additionally, recently in [52], using the Floquet theory and Floquet engineering, it has been found that the QCD vacuum could be altered to a novel state of matter which has been called the “chiral soliton lattice (CSL) of pions”. This has been done by applying a time-periodic circularly polarized laser field which has a large intensity and frequency. The Hamiltonian in these systems can be written as $\mathcal{H}_{\text{total}} = \mathcal{H}_{\pi_0} + \mathcal{H}_{\text{Floquet}}$, where

$$\begin{aligned}\mathcal{H}_{\pi_0} &= \frac{f_\pi^2}{2}(\nabla\pi_0)^2 + m_\pi^2 f_\pi^2(1 - \cos\pi_0), \\ \mathcal{H}_{\text{Floquet}} &= -\lambda \frac{e^2 F^2 f_\pi^2}{3\Omega^3} \partial_z \pi_0,\end{aligned}\quad (5.4)$$

This form of Hamiltonian has been actually observed in various condensed matter systems and high energy physics setups, as mention in [52]. There, it has been pointed out that due to helicity of the laser field, the QCD vacuum would turned into the helical ground state. It would be interesting to study how information-quantity measures would also change under this alternation of vacuum states of QCD. The behavior of Schwinger effect and its connection to entanglement entropy in various setups of electric and magnetic fields which have been studied in [23] could then be employed.

5.3 Holographic neutron stars and quantum information measures

Experimentally, it has been shown that in the regimes with high temperatures, random interactions and spin-exchange collisions, such as in the surface of neutron stars, not all the many-body quantum coherences are destroyed and complex entangled states would still be present. This example could act as a media for probing the properties of the quantum correlations, in the exotic regimes.

In [53], the holographic neutron stars (NS) have been studied where the boundary states are considered as degenerate composite operators which are dual to holographic degenerate stars in the AdS. However, this picture is not complete, as the neutron stars are generally dynamical, periodic and rotating systems and therefore for modeling them, in the boundary system, one should consider a source which is periodically pulsing.

A degenerate state could be constructed using a composite operator in the form of

$$\Phi = \Psi \prod_i \partial_i \Psi \prod_{\{i,j\}} \partial_i \partial_j \Psi \prod_{\{i,j,k\}} \partial_i \partial_j \partial_k \Psi \dots \prod_{\{i_1, i_2, \dots, i_{n_F}\}} \partial_{i_1} \partial_{i_2} \dots \partial_{i_{n_F}} \Psi. \quad (5.5)$$

This is like a set of n_F “shells” which are distinguished by the number of derivatives. The primary operator Ψ would correspond to a fermionic field ψ in the bulk. The quantum correlations between these shells then could be probed by mixed entanglement measures and the phase structure of neutron stars could be constructed. As we showed here that the critical distance D_c could distinguish the scale of chiral breaking/restoration and confinement/deconfinement, it would be a more powerful tool to probe the phase structure of NS, than the entanglement entropy.

In [53], also the critical mass known as Oppenheimer-Volkoff (OV) limit and the Tolman-Oppenheimer-Volkoff (TOV) equation have been discussed. The collapse of a neutron star to a black hole would be dual to a phase transition from a high density (baryonic)

state into a thermal state (quark gluon plasma). The behavior of various quantum measures in such systems during these phase transitions could then be captured by the mixed correlation measures such as EoP and D_c .

The gravitational force could also be simulated by a factor which breaks the coherence and short range entanglement. Therefore, it would expand the range of entanglement which could be modeled by the local quench [7] and MERA, where it can be described by the motion of the dense lump of disentanglers toward the upper directions in the tensor network (TN) models. This picture of TN can also be applied for the neutron star case to numerically construct their phase structures.

The neutron stars can also be modeled using the $T\bar{T}$ deformation of CFT [54] where similar to the confining case, its holographic dual has a cut-off in the bulk geometry side which removes the asymptotic region of AdS and the QFT side would be placed on the Dirichlet wall at a finite radial distance at $r = r_c$, in the bulk side. The results from the studies of $T\bar{T}$ and specifically the new studies of quantum measures in this theory could then be applied for the studies of phase structures of neutron stars and other QCD models

Acknowledgments

I would like to thank Matti Järvinen for supports and helpful discussions. I would also like to thank MDPI publisher for supports in the form of 2019 Universe and 2021 Galaxies travel awards which were helpful in participating various conferences to discuss this work. I am grateful to Prof. Sang Pyo Kim and the organizers of the 17th Italian-Korean symposium for relativistic astrophysics and workshop on cosmology and quantum space time (CQUeST 2021) for their kind invitation. This work has been supported by an appointment to the JRG Program at the APCTP through the Science and Technology Promotion Fund and Lottery Fund of the Korean Government. It has also been supported by the Korean Local Governments – Gyeongsangbuk-do Province and Pohang City – and by the National Research Foundation of Korea (NRF) funded by the Korean government (MSIT) (grant number 2021R1A2C1010834).

References

- [1] S. Ryu and T. Takayanagi, *Holographic derivation of entanglement entropy from AdS/CFT*, *Phys. Rev. Lett.* **96** (2006) 181602, [[hep-th/0603001](#)].
- [2] M. Alishahiha, *Holographic Complexity*, *Phys. Rev. D* **92** (2015), no. 12 126009, [[arXiv:1509.06614](#)].
- [3] A. R. Brown, D. A. Roberts, L. Susskind, B. Swingle, and Y. Zhao, *Holographic Complexity Equals Bulk Action?*, *Phys. Rev. Lett.* **116** (2016), no. 19 191301, [[arXiv:1509.07876](#)].
- [4] M. Ghodrati, *Complexity growth in massive gravity theories, the effects of chirality, and more*, *Phys. Rev. D* **96** (2017), no. 10 106020, [[arXiv:1708.07981](#)].
- [5] M. Ghodrati, *Complexity growth rate during phase transitions*, *Phys. Rev. D* **98** (2018), no. 10 106011, [[arXiv:1808.08164](#)].

- [6] M. Ghodrati, *Complexity and emergence of warped AdS_3 space-time from chiral Liouville action*, *JHEP* **02** (2020) 052, [[arXiv:1911.03819](https://arxiv.org/abs/1911.03819)].
- [7] Y.-T. Zhou, M. Ghodrati, X.-M. Kuang, and J.-P. Wu, *Evolutions of entanglement and complexity after a thermal quench in massive gravity theory*, *Phys. Rev. D* **100** (2019), no. 6 066003, [[arXiv:1907.08453](https://arxiv.org/abs/1907.08453)].
- [8] T. Takayanagi and K. Umemoto, *Entanglement of purification through holographic duality*, *Nature Phys.* **14** (2018), no. 6 573–577, [[arXiv:1708.09393](https://arxiv.org/abs/1708.09393)].
- [9] M. Ghodrati, X.-M. Kuang, B. Wang, C.-Y. Zhang, and Y.-T. Zhou, *The connection between holographic entanglement and complexity of purification*, *JHEP* **09** (2019) 009, [[arXiv:1902.02475](https://arxiv.org/abs/1902.02475)].
- [10] M. Ghodrati, *Entanglement wedge reconstruction and correlation measures in mixed states: Modular flows versus quantum recovery channels*, *Phys. Rev. D* **104** (2021), no. 4 046004, [[arXiv:2012.04386](https://arxiv.org/abs/2012.04386)].
- [11] S. S. Gubser and A. Nellore, *Mimicking the QCD equation of state with a dual black hole*, *Phys. Rev. D* **78** (2008) 086007, [[arXiv:0804.0434](https://arxiv.org/abs/0804.0434)].
- [12] B. Czech, L. Lamprou, S. McCandlish, and J. Sully, *Integral Geometry and Holography*, *JHEP* **10** (2015) 175, [[arXiv:1505.05515](https://arxiv.org/abs/1505.05515)].
- [13] A. Lala, *Entanglement measures for nonconformal D-branes*, *Phys. Rev. D* **102** (2020), no. 12 126026, [[arXiv:2008.06154](https://arxiv.org/abs/2008.06154)].
- [14] P. Jain and S. Mahapatra, *Mixed state entanglement measures as probe for confinement*, *Phys. Rev. D* **102** (2020) 126022, [[arXiv:2010.07702](https://arxiv.org/abs/2010.07702)].
- [15] G. T. Horowitz and R. C. Myers, *The AdS / CFT correspondence and a new positive energy conjecture for general relativity*, *Phys. Rev. D* **59** (1998) 026005, [[hep-th/9808079](https://arxiv.org/abs/hep-th/9808079)].
- [16] M. Ishihara, F.-L. Lin, and B. Ning, *Refined Holographic Entanglement Entropy for the AdS Solitons and AdS black Holes*, *Nucl. Phys.* **B872** (2013) 392–426, [[arXiv:1203.6153](https://arxiv.org/abs/1203.6153)].
- [17] H.-q. Shi and D.-f. Zeng, *Geodesic Motions in AdS Soliton Background Space-time*, [arXiv:1603.08624](https://arxiv.org/abs/1603.08624).
- [18] K. Hashimoto, T. Oka, and A. Sonoda, *Electromagnetic instability in holographic QCD*, *JHEP* **06** (2015) 001, [[arXiv:1412.4254](https://arxiv.org/abs/1412.4254)].
- [19] O. Aharony, J. Sonnenschein, and S. Yankielowicz, *A Holographic model of deconfinement and chiral symmetry restoration*, *Annals Phys.* **322** (2007) 1420–1443, [[hep-th/0604161](https://arxiv.org/abs/hep-th/0604161)].
- [20] J. Maldacena and X.-L. Qi, *Eternal traversable wormhole*, [arXiv:1804.00491](https://arxiv.org/abs/1804.00491).
- [21] T. Numasawa, *Four coupled SYK models and Nearly AdS_2 gravities: Phase Transitions in Traversable wormholes and in Bra-ket wormholes*, [arXiv:2011.12962](https://arxiv.org/abs/2011.12962).
- [22] E. Witten, *Branes and the dynamics of QCD*, *Nucl. Phys. B* **507** (1997) 658–690, [[hep-th/9706109](https://arxiv.org/abs/hep-th/9706109)].
- [23] M. Ghodrati, *Schwinger Effect and Entanglement Entropy in Confining Geometries*, *Phys. Rev. D* **92** (2015), no. 6 065015, [[arXiv:1506.08557](https://arxiv.org/abs/1506.08557)].
- [24] S. K. Domokos and J. A. Harvey, *Baryon number-induced Chern-Simons couplings of vector and axial-vector mesons in holographic QCD*, *Phys. Rev. Lett.* **99** (2007) 141602, [[arXiv:0704.1604](https://arxiv.org/abs/0704.1604)].

[25] I. R. Klebanov and M. J. Strassler, *Supergravity and a confining gauge theory: Duality cascades and chi SB resolution of naked singularities*, *JHEP* **08** (2000) 052, [[hep-th/0007191](#)].

[26] S. S. Gubser and I. R. Klebanov, *Baryons and domain walls in an $N=1$ superconformal gauge theory*, *Phys. Rev. D* **58** (1998) 125025, [[hep-th/9808075](#)].

[27] A. Rolph, *Quantum bit threads*, [arXiv:2105.08072](#).

[28] C. A. Agon and J. F. Pedraza, *Quantum bit threads and holographic entanglement*, [arXiv:2105.08063](#).

[29] P. Basu, D. Das, A. Ghosh, and L. A. Pando Zayas, *Chaos around Holographic Regge Trajectories*, *JHEP* **05** (2012) 077, [[arXiv:1201.5634](#)].

[30] I. Bena, A. Buchel, and O. J. C. Dias, *Horizons cannot save the Landscape*, *Phys. Rev. D* **87** (2013), no. 6 063012, [[arXiv:1212.5162](#)].

[31] D. Kaviani and A. E. Mosaffa, *Temperature in the Throat*, *Nucl. Phys. B* **910** (2016) 724–753, [[arXiv:1503.02026](#)].

[32] J. M. Maldacena and C. Nunez, *Towards the large N limit of pure $N=1$ superYang-Mills*, *Phys. Rev. Lett.* **86** (2001) 588–591, [[hep-th/0008001](#)].

[33] N. Evans and J. Mitchell, *Domain Wall AdS/QCD*, [arXiv:2108.12152](#).

[34] R. A. Janik, M. Jarvinen, and J. Sonnenschein, *A simple description of holographic domain walls in confining theories — extended hydrodynamics*, *JHEP* **09** (2021) 129, [[arXiv:2106.02642](#)].

[35] M. Bianchi, D. Consoli, A. Grillo, and J. F. Morales, *More on the SW-QNM correspondence*, [arXiv:2109.09804](#).

[36] J. Kumar Basak, H. Parihar, B. Paul, and G. Sengupta, *Holographic entanglement negativity for disjoint subsystems in $\text{AdS}_{d+1}/\text{CFT}_d$* , [arXiv:2001.10534](#).

[37] J. Evslin and L. Martucci, *D-brane networks in flux vacua, generalized cycles and calibrations*, *JHEP* **07** (2007) 040, [[hep-th/0703129](#)].

[38] D. Lust, F. Marchesano, L. Martucci, and D. Tsimpis, *Generalized non-supersymmetric flux vacua*, *JHEP* **11** (2008) 021, [[arXiv:0807.4540](#)].

[39] P. Koerber and L. Martucci, *Deformations of calibrated D-branes in flux generalized complex manifolds*, *JHEP* **12** (2006) 062, [[hep-th/0610044](#)].

[40] I. Bakhmatov, N. S. Deger, J. Gutowski, E. Ó. Colgáin, and H. Yavartanoo, *Calibrated Entanglement Entropy*, *JHEP* **07** (2017) 117, [[arXiv:1705.08319](#)].

[41] J. F. Pedraza, A. Russo, A. Svesko, and Z. Weller-Davies, *Lorentzian threads as 'gatelines' and holographic complexity*, [arXiv:2105.12735](#).

[42] J. F. Pedraza, A. Russo, A. Svesko, and Z. Weller-Davies, *Sewing spacetime with Lorentzian threads: complexity and the emergence of time in quantum gravity*, [arXiv:2106.12585](#).

[43] Q. Wen, *Balanced Partial Entanglement and the Entanglement Wedge Cross Section*, *JHEP* **04** (2021) 301, [[arXiv:2103.00415](#)].

[44] M. Han and Q. Wen, *First Law and Quantum Correction for Holographic Entanglement Contour*, [arXiv:2106.12397](#).

- [45] B. Czech, L. Lamprou, S. Mccandlish, and J. Sully, *Modular Berry Connection for Entangled Subregions in AdS/CFT*, *Phys. Rev. Lett.* **120** (2018), no. 9 091601, [[arXiv:1712.07123](https://arxiv.org/abs/1712.07123)].
- [46] R. Penner *Commun. Math. Phys.* **113** 299–339 (1987).
- [47] B. Boldis and P. Lévy, *Cluster algebraic description of entanglement patterns for the BTZ black hole*, [arXiv:2108.10638](https://arxiv.org/abs/2108.10638).
- [48] D. S. Ageev, *Shaping contours of entanglement islands in BCFT*, [arXiv:2107.09083](https://arxiv.org/abs/2107.09083).
- [49] N. Bao, J. Harper, and G. N. Remmen, *Holevo Information of Black Hole Mesostates*, [arXiv:2103.06888](https://arxiv.org/abs/2103.06888).
- [50] M. Hanada, *Bulk geometry in gauge/gravity duality and color degrees of freedom*, [arXiv:2102.08982](https://arxiv.org/abs/2102.08982).
- [51] A. Tomiya and Y. Nagai, *Gauge covariant neural network for 4 dimensional non-abelian gauge theory*, [arXiv:2103.11965](https://arxiv.org/abs/2103.11965).
- [52] A. Yamada and N. Yamamoto, *Floquet vacuum engineering: laser-driven chiral soliton lattice in the QCD vacuum*, [arXiv:2107.07074](https://arxiv.org/abs/2107.07074).
- [53] J. de Boer, K. Papadodimas, and E. Verlinde, *Holographic Neutron Stars*, *JHEP* **10** (2010) 020, [[arXiv:0907.2695](https://arxiv.org/abs/0907.2695)].
- [54] F. A. Smirnov and A. B. Zamolodchikov, *On space of integrable quantum field theories*, *Nucl. Phys. B* **915** (2017) 363–383, [[arXiv:1608.05499](https://arxiv.org/abs/1608.05499)].